



Hydrogen Gas Promoted Self-Limiting Copper Monolayer Deposition on Platinum

Paulette A. Loichet Torres,^{*,z}  Hany A. El-Sayed,^{ib}  Jan N. Schwämmlein,^{ib} 
Franziska Friedrich,^{*}  and Hubert A. Gasteiger^{**} 

Chair of Technical Electrochemistry, Department of Chemistry and Catalysis Research Center, Technical University of Munich, D-85748 Garching, Germany

A hydrogen gas promoted approach to achieve copper underpotential deposition (UPD) on platinum surfaces was developed to form a copper monolayer on polycrystalline platinum and carbon supported platinum catalysts (Pt/C) in a Cu²⁺-containing electrolyte, serving as alternative to the commonly used electrochemical deposition methods that require external potential control. Initially, the amount of deposited copper in the presence of dissolved hydrogen was determined via fast stripping voltammetry. Subsequently, by monitoring the open circuit potential drop of Pt disk and Pt/C thin-film electrodes upon exposure of an air saturated electrolyte to H₂ containing gas, it could be shown that self-limiting Cu coverages of essentially one monolayer can reliably be obtained for 0.1% and 3% H₂/Ar mixtures. In a second part, a cell was designed aiming to facilitate the gram-scale preparation of Cu_{UPD}Pt/C catalysts by the H₂ gas promoted approach. The formation of a Cu UPD layer on the Pt nanoparticles supported on carbon with a coverage slightly higher than a monolayer was successfully validated. However, the reaction cell introduced non-idealities at the solution/gas interface, which would need to be optimized to achieve a perfectly self-limiting Cu monolayer on the Pt nanoparticles by the H₂ promoted deposition.

© 2021 The Author(s). Published on behalf of The Electrochemical Society by IOP Publishing Limited. This is an open access article distributed under the terms of the Creative Commons Attribution 4.0 License (CC BY, <http://creativecommons.org/licenses/by/4.0/>), which permits unrestricted reuse of the work in any medium, provided the original work is properly cited. [DOI: 10.1149/1945-7111/abfe79]



Manuscript submitted March 16, 2021; revised manuscript received May 2, 2021. Published May 27, 2021.

Even though proton exchange membrane fuel cells (PEM-FCs) represent a very promising alternative to combustion engines, drawbacks such as the need for a renewable H₂ infrastructure together with the high cost of Pt metal, used as a catalyst in the PEM-FC electrodes, have hindered its implementation.^{1,2} Efforts are currently being made in the development of highly active fuel cell electrocatalysts to reduce the Pt loading in the membrane electrode assemblies (MEAs) and consequently reduce the cost of the stack, with a focus on catalysts for the oxygen reduction reaction (ORR),^{2–7} since the ORR overpotential accounts for most of the voltage and efficiency losses in a PEM-FC.

Over the last decades, newly developed bimetallic ORR catalysts have been reported to have a remarkable increase in activity compared to pure Pt.^{3–8} Some successful attempts in the preparation of these highly active catalysts include the formation of core-shell like structures, consisting of a Pt monolayer (ML) shell covering a metal (M = Pd, Au) or metal-alloy (M_{alloy} = Co-Pd, Ir-Re, Ni-Au) core.^{9–14} In these core/ML-shell catalysts, the interaction between the Pt shell and the metal(-alloy) core causes a strain on the Pt layer that favorably modifies its ability to bind the reaction intermediates of the ORR,^{9,11,14} resulting in catalyst materials such as the Pt_{ML}/Pd/C reported to present a ~5-fold mass activity enhancement compared to a commercial Pt/C catalyst.¹⁵ To form the desired Pt monolayer shell, however, controlled deposition methods are required. The Adzić group that pioneered this catalyst concept used a synthesis method involving the initial electrochemical deposition of a Cu monolayer onto a variety of core materials, followed by a subsequent deposition of Pt onto the core material via the galvanic displacement of the Cu atoms.^{9,12,14,16} Based on a similar principle, Pt near-surface alloys (NSAs) have also been developed as highly active ORR catalysts. Specifically, Cu-Pt NSAs were prepared as bulk electrodes by electrochemically depositing a Cu monolayer onto a Pt(111) single-crystal substrate, after which a short high-temperature treatment was shown to lead to the formation of a Cu/Pt(111) near-surface alloy.^{17–20} In one instance, the ORR activity of a Cu/Pt(111) NSA resulted in an 8-fold increase in ORR activity compared to a Pt(111) electrode at 0.9 V.²⁰ Clearly, our interest on

the formation of a Cu monolayer by the underpotential deposition of Cu (Cu_{UPD}) on a core metal (alloy) is based on the important role that the Cu_{UPD} has in the preparation of novel ORR catalysts, as it is the proposed initial step in the synthesis of many core/ML-shell and NSA based catalysts. However, in most cases, the deposition of a Cu_{UPD} layer requires external potential control of the core material/substrate, which is straightforward when using bulk core material electrodes or nanoparticle core materials (either supported on carbon or unsupported) that can be attached onto a rotating disk electrode (RDE).^{10,15} While the latter approach was used to produce milligram-quantities of carbon supported core/ML-shell catalysts that could then be tested in actual PEM fuel cells,²¹ the preparation of gram-quantities or even a larger scale for an industrial application requires different approaches. One of the first scale-up capable syntheses was proposed by Sasaki et al., who have designed an electrochemical cell to deposit Cu monolayers on gram-quantities of core nanoparticles supported on carbon (core/C), whereby the core/C nanoparticles are dispersed in a Cu²⁺-containing electrolyte that is being stirred in an electrochemical reactor with a cylindrical titanium electrode that is polarized to the Cu_{UPD} potential of the core material.¹⁵ Although the technique represents a very promising approach into the preparation of gram quantities of so-called Pt monolayer catalysts, the Cu deposition step is still limited by a potential control with an external potentiostat, which could hinder the upscaling of the method for the industrial-level production of these catalysts.

Purely chemically controlled reaction routes for Cu_{UPD} formation as an alternative to the electrochemically controlled deposition were also explored by Szabo et al.^{22–26} They proposed the chemical deposition of Cu (as well as Ag, Bi, and Au) on polycrystalline Pd and Pt electrodes by the displacement of hydrogen atoms on the surface of the Pd and Pt substrate electrodes. Via this technique, the underpotential deposition of hydrogen (H_{UPD}) is either formed via external potential control or produced on the Pt or Pd electrode by saturating the acidic electrolyte with hydrogen gas that leads to a polarization of the Pt or Pd electrode to near 0 V vs the reversible hydrogen electrode (RHE) potential. Subsequently, the electrolyte is exchanged with an acidic electrolyte that contains the desired foreign metal ion, promoting in most cases the bulk deposition of the foreign metal. The dissolution of the bulk deposits is reported to leave behind an adsorbed layer of the foreign metal on the Pt or Pd electrode substrate similar to the one obtained by electrochemical

*Electrochemical Society Student Member.

**Electrochemical Society Fellow.

^zE-mail: paulette.loichet@tum.de

methods.²² The tailoring of the desired compositions on the substrate surface have been achieved by restricting the initial amount of the precursors or by removing the ion-containing solution; yielding coverages from sub-monolayers to several layers on the polycrystalline Pt or Pd electrode substrates. Variants of this method were also used in the deposition of Pd and Rh ad-layers on Pt single crystal electrodes by the so-called “force deposition” technique, in which a droplet of the desired foreign metal ion solution is set on top of the Pt single crystal. The reduction of the metal ions is promoted by the careful immersion of the solution-covered electrodes into a bubbler containing H₂/Ar saturated water. In this approach, the desired metal coverages were controlled by the concentration of the metal ions in the droplet.^{27–29}

Moreover, these chemically controlled reaction routes have also been implemented in the preparation of oxide supported catalysts for heterogeneous catalysis applications, whereby oxide supported nanoparticles that form H_{UPD} (e.g., Pt, Pd, etc.) were immersed into a hydrogen gas saturated electrolyte that contained defined and limited amounts of a second active metal that would deposit under these conditions either by H_{UPD} displacement or simply on account of the near 0 V vs RHE potential that is established on platinum group metals in contact with H₂ saturated electrolyte. This way, a variety of alloy nanoparticle catalysts of Pd–Pt, Cu–Rh, and Au–M₁ (M₁ = Pt, Pd and Rh) were prepared.^{30–32} In a similar manner, carbon supported Pd particles with a Pt monolayer shell were prepared by adding an aqueous CuCl₂ solution to a H₂ saturated dispersion of carbon supported Pd (Pd/C) in ethanol/water, whereby the authors suggest that adsorbed UPD hydrogen undergoes a redox reaction with the Cu²⁺ ions to form a Cu ML.³³

In the following, we will explore the viability of the H₂ gas promoted formation of a Cu_{UPD} monolayer on a Pt/C catalyst that in principle is amenable to large-scale processing and thus could serve as an initial step in the synthesis of Cu–Pt NSAs and core/ML-shell catalysts. In contrast to common Cu_{UPD} techniques that require potential control to establish a copper monolayer, the presented Cu deposition method on the different Pt surfaces is solely controlled by the introduction of a H₂ gas mixture into a Cu²⁺ containing electrolyte. Thus, it would provide a synthesis route without the need of an external potentiostat, which could be employed not only in the formation of a Cu_{UPD} monolayer on a Pt surface but could further be adapted in the preparation of relevant core/ML-shell catalysts with cores from the platinum metal group.

In our work, we will first examine the potential-dependent Cu_{UPD} formation on a bulk Pt disk and the quantification of the copper coverage by fast stripping voltammetry in a RDE set-up. The potential-dependent Cu_{UPD} formation will then be compared to the Cu coverage on a Pt disk that is obtained when saturating the Cu²⁺-containing electrolyte with H₂/Ar gas mixtures at open circuit potential (OCP) conditions, i.e., without external potential control of the Pt disk. Following the change of the OCP of the Pt disk, one can show that for an optimized H₂ concentration the disk potential gradually decreases to the potential expected for a Cu_{UPD} monolayer; the formation of a Cu_{UPD} monolayer in this case will be proven by fast stripping voltammetry. Subsequently, we show that a Cu_{UPD} monolayer can be produced by the same method on the Pt nanoparticles of a Pt/C catalyst attached to a glassy carbon rotating disk electrode. Finally, using a specially designed cell, we will evaluate the gram-scale preparation of a Cu_{UPD} monolayer on Pt/C catalysts by this H₂ gas promoted copper deposition approach.

Experimental

Preparation of the electrolyte solution.—A 0.1 M HClO₄ solution was obtained from the dilution of a 60% HClO₄ stock solution (Cica Reagent, Kanto Chemical Co., INC., Japan) using ultra-pure water with a specific resistance of 18.2 MΩ cm (Milli-Q Integral 5, Merck-MilliPore, Germany). To prepare the Cu²⁺-containing electrolyte, CuO (99.999%, Sigma Aldrich Corp., Germany) was

directly mixed with the 60% HClO₄ solution and stirred at 60 °C until completely dissolved. The resulting blue solution was diluted to obtain a 1 mM, 10 mM, or 20 mM Cu²⁺ in 0.1 M HClO₄. The HClO₄ present in the prepared Cu²⁺-containing solutions acted as supporting electrolyte for the evaluation of the electrochemical Cu deposition and the determination of the Cu coverage by fast stripping CVs. In order to have a valid comparison between the RDE results and the gram-scale H₂ gas promoted Cu_{UPD}, both experiments were performed using the same proton activity (i.e., for a 0.1 M HClO₄ electrolyte with $a_{H^+} \approx 0.1$ and pH ≈ 1). However, the effect of the pH on the here developed H₂ gas promoted Cu_{UPD} was briefly evaluated by reducing the electrolyte concentration to 0.01 M HClO₄ (with $a_{H^+} \approx 0.01$ and pH ≈ 2 ; experiment not shown) in an RDE set-up, resulting in a similar Cu_{UPD} deposition process as the experiments performed in the lower pH solutions. Overall, we observed that under the evaluated acidic conditions the H₂ gas promoted deposition was significantly more sensitive to the H₂ gas concentration than to the pH, as will be shown in the proposed mechanism discussed in the following sections.

Pt disk and Pt/C thin-film rotating disk electrode preparation.—

A Pt, Cu, or glassy carbon (GC) disk (5 mm diameter in an E5 or E6 electrode tip, Pine Research Instrumentation, USA) supported on a rotating disk electrode (RDE) shaft (AFE6M, Pine Research Instrumentation, USA) was used as working electrode (WE) for RDE experiments. Prior to the measurements, the disks were polished with a 0.05 μm alumina suspension (Bühler AG, Germany). The electrodes were then ultra-sonicated (USC100T, VWR International GmbH, Germany) in ultra-pure water (3x) before they were introduced into the electrolyte solution for their electrochemical characterization.

The GC disk was employed as substrate for the Pt/C thin-film electrodes. For these, a catalyst ink with a concentration of 2 mg_{catalyst} ml⁻¹ was prepared by dispersing 4 mg of a 46.1 wt% Pt/C catalyst (TEC10EA50E, Tanaka Kikinokogyo K.K., Japan) in 2 ml of (7:3 ml:ml) H₂O:isopropanol (Chromasolv Plus, 99.9%, Sigma Aldrich Corp., Germany). The slurry was then sonicated for 20 min, after which, 2 μl of Nafion® (5 wt% Nafion® in lower aliphatic alcohols with 15%–20% H₂O, Sigma Aldrich Corp., Germany) were added; yielding an ionomer to carbon mass ratio of 0.04/1. The small amount of Nafion® was used to insure the stability of the electrode coatings during the experiments, and was shown not to affect the Cu deposition. After 10 more minutes of sonication, 7 μl of the prepared ink was drop-cast onto the cleaned GC disk and set to dry under air, resulting in a calculated Pt loading of $\sim 33 \mu\text{g}_{\text{Pt}} \text{cm}^{-2}_{\text{disk}}$ or a total Pt amount of $\sim 6.5 \mu\text{g}_{\text{Pt}}$ on the glassy carbon disk substrate.

Electrochemical measurements with Pt and Pt/C thin-film RDEs.—

The electrochemical experiments were performed in a three-electrode glass cell design, comprised of (i) the corresponding working electrode (WE) immersed in the electrolyte in the WE compartment; (ii) a platinum mesh as counter electrode (CE), separated from the WE compartment by a porous glass frit; and (iii) a static reversible hydrogen electrode (RHE) as reference electrode (RE), connected to the cell by a Luggin capillary. All potentials in this work are referred to the RHE scale; the RHE reference electrode consisted of a small 0.1 M HClO₄ filled tube with a sealed-in Pt wire on one end and a small capillary connecting to the electrolyte of the cell on the other end, whereby a small H₂ gas bubble was formed prior to the experiments on the RE Pt-wire, yielding a so-called static RHE, as described previously.³⁴ The measurements were carried out using an Autolab potentiostat (PGSTAT302N, Metrohm AG, Switzerland).

Before each measurement, the Pt and the Pt/C thin-film electrodes were electrochemically cleaned in the Cu-free electrolyte solution under Ar atmosphere. The procedure consisted of cycling the potential between 0.05 V_{RHE} and 1.3 V_{RHE} at 200 mV s⁻¹ until

no further changes in the cyclic voltammogram (CV) features were observed. Then, three additional cycles were recorded over the same potential range at 10 mV s^{-1} , and the surface area of the electrodes was estimated from the last cycle of these CVs. To do so, the charge associated with the hydrogen underpotential deposition (H_{UPD}) region was extracted and the Pt surface area was calculated by considering a specific H_{UPD} charge of $210 \mu\text{C cm}^{-2}$. The thus determined roughness factor for the Pt disk electrode was $1.3 \text{ cm}^2_{\text{Pt}} \text{ cm}^{-2}_{\text{disk}}$, while that for the Pt/C thin-film RDE was $18 \text{ cm}^2_{\text{Pt}} \text{ cm}^{-2}_{\text{disk}}$ (corresponding to a Pt specific surface area of $55 \pm 1 \text{ m}^2_{\text{Pt}} \text{ g}^{-1}_{\text{Pt}}$ for the Pt/C catalyst).

To study the electrochemical deposition of Cu on Pt, the WE was immersed in the Cu^{2+} -containing electrolyte solution, where a set of CVs were recorded at different scan rates, while the electrode was rotated at 400 rpm in all cases. The Cu coverages (θ_{Cu}) were calculated from the third CV of each set by the integration of the anodic region of the voltammograms ($Q_{\text{Cu}_{\text{anodic}}}$) and further normalization by the charge associated to the H_{UPD} features ($Q_{H_{\text{UPD}}}$), as shown in Eq. 1 and considering the specific charge for the 2 electron Cu deposition process on a polycrystalline Pt disk to be equal to $420 \mu\text{C cm}^{-2}$.³⁵

$$\theta_{\text{Cu}} = \frac{Q_{\text{Cu}_{\text{anodic}}}}{2Q_{H_{\text{UPD}}}} \quad [1]$$

Hydrogen gas promoted Cu deposition on the Pt disk and the Pt/C thin-film electrodes.—The initially Ar-purged Cu^{2+} -free and Cu^{2+} -containing electrolytes were purged with different concentrations of H_2 to evaluate the extent of Cu deposition on the Pt disk and on the Pt/C thin-film working electrodes, using the above described RDE setup and a rotation rate of 1600 rpm, in order to allow for a fast mass transport of Cu^{2+} ions to the WEs. The open circuit potential (OCP) transients of the working electrodes were recorded over the course of the H_2 purge, using a multimeter (289 True RMS Data Logging Multimeter, Fluke Corporation, USA) connected between the WE and the RE. Three different concentrations of H_2 were employed in this study, namely 100% H_2 (grade 6.0, Westfalen AG, Germany) as well as 0.1% and 3% H_2 in Ar mixtures (H_2 and Ar both grade 6.0, Westfalen AG, Germany). The H_2 gas was purged through the respective electrolyte solutions with a flow rate of 40 l h^{-1} . After the chosen Cu deposition time, the WE, CE, and RE were connected to the potentiostat to strip the deposited Cu by stripping voltammetry. Stripping CVs were recorded in the absence of rotation, starting from the OCP and scanning to $1.2 \text{ V}_{\text{RHE}}$ at 100 mV s^{-1} while still purging the electrolyte with hydrogen in order to prevent a positive shift of the OCP that could result in a partial dissolution and/or oxidation of the deposited Cu. The high stripping scan rate was specifically selected to avoid any significant contribution of the hydrogen oxidation reaction on the stripping CV charge, which is the case when using 0.1% and 3% H_2 in Ar mixtures due to the slow H_2 mass transport in the absence of rotation.

Large-scale synthesis for carbon supported $\text{Cu}_{\text{UPD}}\text{Pt/C}$ materials.—A reaction cell was designed to enable the H_2 gas promoted deposition of a Cu_{UPD} layer on the Pt nanoparticles of a carbon supported Pt catalyst (referred to as $\text{Cu}_{\text{UPD}}\text{Pt/C}$). The cell setup was designed to allow for both the underpotential deposition of Cu and the collection of the resulting $\text{Cu}_{\text{UPD}}\text{Pt/C}$ under a H_2 -containing gas flow purging the electrolyte. Two deposition experiments were evaluated in the Cu deposition configuration, presented in Fig. 1a: a first deposition with 0.5 g of a 46.1 wt% Pt/C catalyst dispersed in 80 ml of a 10 mM Cu^{2+} in 0.1 M HClO_4 electrolyte, and a second experiment with 0.5 g of a 20.0 wt% Pt/C catalyst (TEC10V20E, Tanaka Kikinokogyo K.K., Japan) dispersed in 110 ml of a 5 mM Cu^{2+} in 0.1 M HClO_4 electrolyte. To start the Cu deposition, a

5% H_2/Ar mixture (H_2 and Ar both of grade 6.0, Westfalen AG, Germany) was bubbled through the Pt/C dispersion at a flow rate of 10 l h^{-1} . An RHE reference electrode (as described above) was used to monitor the OCP of a Pt-wire sensing electrode (SE) via a multimeter (289 True RMS Data Logging Multimeter, Fluke Corporation, USA), providing a measure of the effective potential of the Pt/C particles. Throughout the H_2 promoted deposition, the catalyst was stirred with a magnetic stirrer.

Once the Cu underpotential deposition reaction was completed, the cell setup was turned upside-down into the configuration where the $\text{Cu}_{\text{UPD}}\text{Pt/C}$ could be collected under a H_2 -containing environment (shown in Fig. 1b). The $\text{Cu}_{\text{UPD}}\text{Pt/C}$ particles were collected on a filter paper (Supor® 0.2 μm PES, Pall Corporation, USA) secured on a porous frit at the bottom part of the cell in this configuration. During this step, the outlet at the bottom of the cell was connected to a pump for vacuum filtration while the cell was kept under a continuously purged H_2 -containing gas atmosphere. The removed electrolyte solution was analyzed directly after the initial filtration for its copper content by UV-vis (Lambda35, Perkin Elmer, USA). Subsequently, the catalyst was washed with H_2 -saturated water to ensure the complete removal of any residual Cu^{2+} -containing electrolyte, and the resulting nanoparticles were left to dry at 80°C under the hydrogen purge. The composition of the as-synthesized $\text{Cu}_{\text{UPD}}\text{Pt/C}$ materials was determined by elemental analysis; where the Cu content was obtained using atomic absorption (AA280 FS, Agilent, USA) and the Pt content was determined by photometry (Cary 100 (410 nm), Agilent, USA).

Results and Discussion

Potentiodynamic Cu_{UPD} formation on polycrystalline Pt disk electrodes.—An initial study was performed with a Pt disk WE to determine the Cu coverage as a function of the applied potential and the deposition scan rate under potentiodynamic conditions. Cathodic potential scans recorded in the Cu^{2+} containing electrolytes, starting from $1.3 \text{ V}_{\text{RHE}}$ to lower potentials, were selected over other electrochemical deposition techniques (e.g., potential step) to serve as a reference point when describing the H_2 gas promoted Cu deposition on the Pt/C catalyst, while the anodic potential scans were evaluated to define the adequate stripping parameters required to estimate the amount of Cu deposited on the Pt surface.

For the study of the electrochemical deposition of Cu, a set of CVs at different scan rates and at 400 rpm were recorded at a constant positive (anodic) potential limit of $1.3 \text{ V}_{\text{RHE}}$, while successively decreasing the negative (cathodic) potential limit. The well-known characteristic Pt H_{UPD} features and the Pt-oxide formation/reduction features obtained in a Cu-free 0.1 M HClO_4 electrolyte can be observed from the solid black curves in Fig. 2 and are essentially identical for the here used scan rates. On the other hand, for the CVs in the electrolyte containing 1 mM Cu^{2+} , the Cu underpotential deposition features strongly depend on the scan rate, moving to more negative potentials with increasing scan rates, as shown in Figs. 2a–2c. Comparable results have been described previously, where the strong dependence of the Cu deposition on the scan rate was attributed to the slow kinetics of the deposition process.^{36,37}

In the following, we will discuss in detail the CVs in the 0.1 M HClO_4 electrolyte with 1 mM Cu^{2+} . At the slowest scan rate of 5 mV s^{-1} (Fig. 2a), all CVs converge to the same peak for the cathodic scan in the range between 0.8 – $1.3 \text{ V}_{\text{RHE}}$ (marked as section I), which is attributed to the reduction of Pt-oxide.^{35,38} At potentials between 0.3 – $0.8 \text{ V}_{\text{RHE}}$ (marked as section II), a set of broad peaks is observed that represent the underpotential deposition of Cu, ending just positive of $\sim 0.3 \text{ V}_{\text{RHE}}$ at this scan rate of 5 mV s^{-1} . At potentials below $\sim 0.3 \text{ V}_{\text{RHE}}$, the onset of Cu bulk deposition is evidenced by a sharp increase of the cathodic current (marked as section III).^{35,37,39,40} In agreement with previous studies, the H_{UPD} features do not appear, as Cu ad-atoms have been found to hinder the adsorption of hydrogen on the Pt surface.^{38,41,42} The completion of

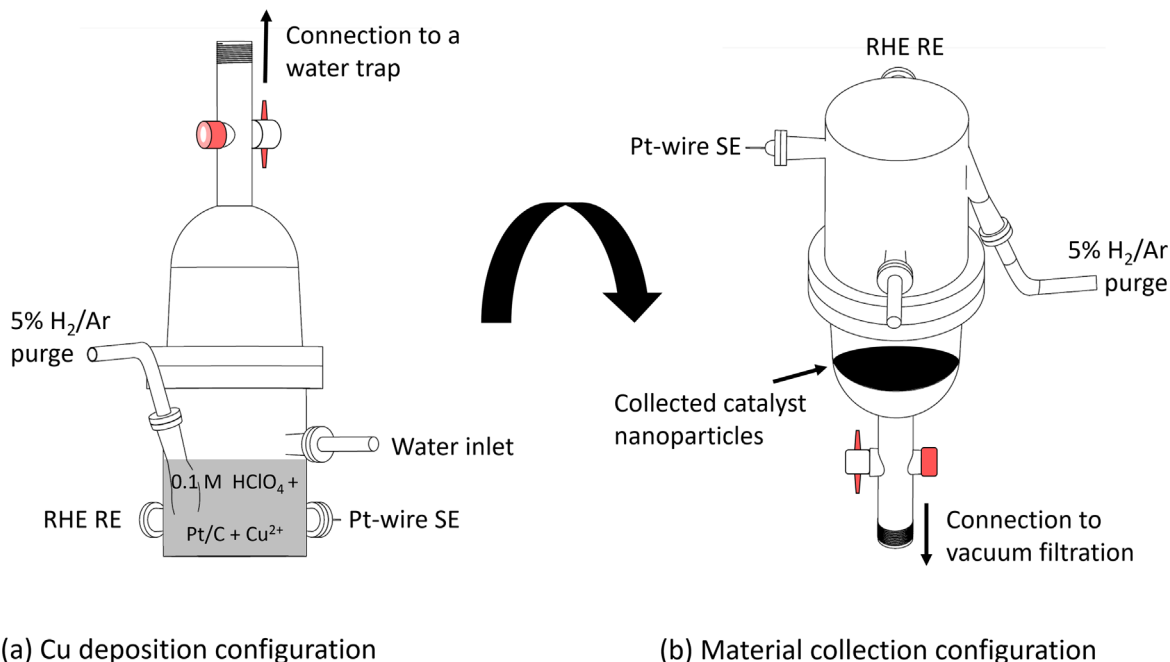


Figure 1. Reaction cell for the H₂ gas promoted deposition of a Cu monolayer on a Pt/C catalyst and the subsequent collection of the thus produced Cu_{UPD}Pt/C material under a continuously purged hydrogen containing gas atmosphere. (a) Cell setup configuration during the deposition of Cu on the Pt/C catalyst dispersed in a Cu²⁺-containing 0.1 M HClO₄ electrolyte that is purged with 5% H₂/Ar; the effective potential of the Pt/C catalyst is monitored by the potential of a Pt-wire sensing electrode (SE) measured vs an RHE reference electrode (RE). (b) Turned upside-down cell setup configuration used to wash and collect the formed Cu_{UPD}Pt/C material under hydrogen atmosphere.

the Cu_{UPD} layer is indicated by the inflection point at $\sim 0.35 V_{RHE}$ at 5 mV s^{-1} , as will be demonstrated more quantitatively by the deposition charge analysis shown later (Fig. 3). Looking at the subsequent anodic (i.e., positive-going) scan, a small anodic peak (at $0.3 V_{RHE}$) appears for cathodic potential windows opened to $\leq 0.25 V_{RHE}$. This peak is only seen after the deposition of bulk Cu and is clearly related to the oxidation of bulk/multi-layer Cu deposits. At more positive potentials, three distinct peaks (at 0.5, 0.68, and $0.76 V_{RHE}$) due to the oxidative stripping of Cu ad-atoms at different adsorption energies are identified.^{35,38} At even more positive potentials, a comparison of the CV with (blue lines) and without Cu²⁺ in the solution (black line) clearly shows that the onset potential of Pt oxidation is shifted positively in the presence of Cu ad-atoms, corresponding to a suppression of Pt oxide formation in an analogous way as for the H-adsorption. At $> 1 V_{RHE}$ however, all the curves merge, indicating that all Cu ad-atoms have been stripped from the Pt surface.

Comparing Figs. 2a and 2b recorded at 5 and 10 mV s^{-1} , respectively, the same onset potential is observed for the Cu_{UPD} process, while the completion of the Cu_{UPD} layer and the onset of bulk Cu deposition are shifted to lower potentials at the higher scan rate. The negative shift of the Cu_{UPD} and the Cu bulk deposition features with increasing scan rate is even more pronounced at 100 mV s^{-1} (Fig. 2c), where despite the fact that two Cu stripping peaks are observed, no significant reduction features are observed until approximately $0.35 V_{RHE}$, in which the Cu_{UPD} is evidenced by the peak at $0.25 V_{RHE}$. This behavior clearly exemplifies the dependence of the Cu deposition on the scan rate, indicating that the deposition of Cu is a relatively slow process.^{35,36} (note that the limiting current for Cu²⁺ to the disk at the here used concentration of 1 mM Cu^{2+} and 400 rpm is estimated to be on the order of 0.7 mA cm^{-2} ,³⁶ which would be able to provide a full Cu_{UPD} layer within $\ll 1 \text{ s}$, i.e., within a voltage window of $\ll 100 \text{ mV}$ at 100 mV s^{-1}). Thus, the slow Cu deposition kinetics lead to an only partially Cu covered Pt surface at 100 mV s^{-1} , which is also apparent by the clearly smaller Cu_{UPD} stripping features in Fig. 2c, compared to Figs. 2a and 2b.

To quantify the Cu_{UPD} coverage as a function of the cathodic potential limit and of the applied scan rate, a commonly used analysis method based on Cu_{UPD} stripping voltammetry was used, i.e., integrating the Cu stripping peaks and subtracting the background CV charge obtained in a Cu²⁺-free electrolyte in the same potential range.^{35,38,39} Figure 3a outlines the here adopted integration and background subtraction procedure, illustrated for the Cu_{UPD} stripping region for three of the CVs recorded at 5 mV s^{-1} (from Fig. 2a) in 0.1 M HClO₄ both without Cu²⁺ (black line) and with 1 mM Cu^{2+} (blue lines). A closer look into these curves shows that a simple subtraction of the charge between the two curves in the different electrolytes (solid blue and black lines, Fig. 3a), yielding the light gray area, would underestimate the Cu coverage. In this case, the charge originating from the Pt oxidation in the Cu²⁺-free electrolyte from $0.5 V_{RHE}$ to $\sim 0.83 V_{RHE}$ would be subtracted from the Cu_{UPD} stripping charge (dark gray area, Fig. 3a), even though the Pt oxide onset is clearly shifted to potentials higher than $\sim 0.85 V_{RHE}$ in the presence of Cu_{UPD} on the Pt electrode. To avoid this obvious underestimation of the Cu coverage, a new base line was constructed as represented by the black dashed lines in Fig. 3a. To begin with, a horizontal line based on the double layer charge of the base CV without Cu²⁺ ions (labeled as (1)) was extended until the onset of Pt-oxide formation in the base CV (labeled as (2)), from which another line was extended to connect point (2) with the inflection point of the CV in the Cu²⁺-containing electrolyte (labeled as (3)). The Cu_{UPD} charge was then estimated as the charge corresponding to the area between the thus constructed dashed black lines and the CV features in the presence of Cu²⁺ ions (blue curve). While this also is only an approximation of the true Cu_{UPD} charge, we believe it is more closely reflecting the actual Cu_{UPD} charge rather than the charge that would be obtained by a simple subtraction of the base CV from the CV in the presence of Cu²⁺ ions.

Figure 3b shows the thus determined Cu_{UPD} coverages for the CVs shown in Fig. 2 and analyzed according to Fig. 3a as a function of the cathodic potential limit and of the scan rate. The trend observed for all experiments is an increase of the Cu coverage on the Pt surface with decreasing cathodic potential limits. At the fastest scan rate of 100 mV s^{-1} , the Cu coverage only reaches ~ 0.54 monolayers for the CV with the lowest measured cathodic limit of $0.1 V_{RHE}$ (green symbols

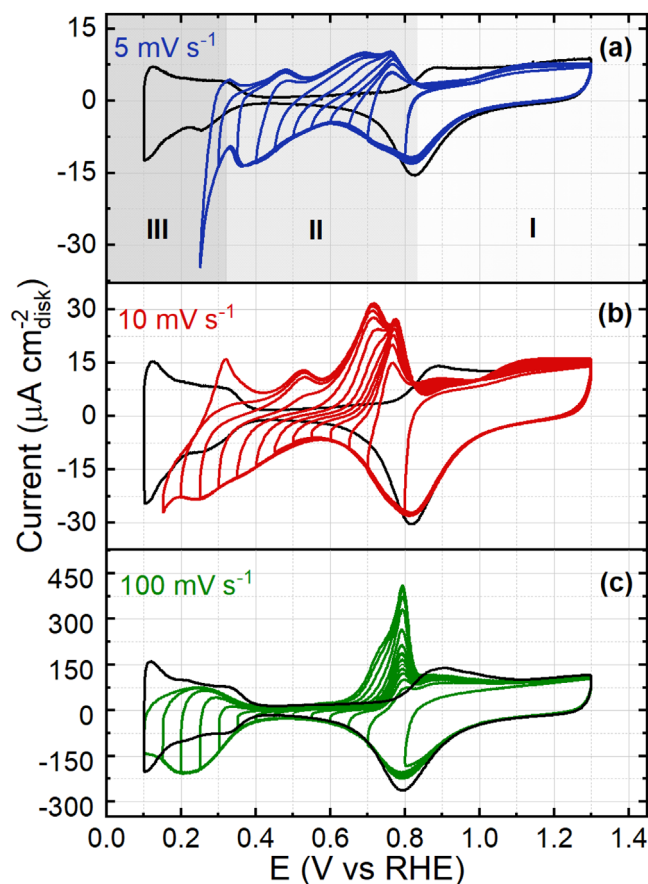


Figure 2. CVs of a Pt RDE (400 rpm, under Ar purge) in 0.1 M HClO₄ electrolyte with 1 mM Cu²⁺, recorded with a positive potential limit of 1.3 V_{RHE} and with negative potential limits decreasing from 0.8 V_{RHE} to 0.1 V_{RHE} in 0.05 V steps at different scan rates: (a) 5 mV s⁻¹ (blue), (b) 10 mV s⁻¹ (red), and (c) 100 mV s⁻¹ (green). The shown CVs correspond to the 3rd cycle for each negative potential limit; for reference, the black lines show the CVs in Cu-free 0.1 M HClO₄ between 1.3 and 0.1 V_{RHE}.

in Fig. 3b), due to the slow Cu_{UPD} and Cu bulk deposition process on Pt in HClO₄ electrolyte.³⁶ On the other hand, for the slower scan rates of 5 and 10 mV s⁻¹, full monolayer coverages are achieved at 0.35 V_{RHE} and 0.25 V_{RHE} respectively, indicated by the gray dotted line in Fig. 3b. This corresponds closely to the inflection point of the cathodic scans just before the onset of the Cu bulk deposition/stripping features in Figs. 2a and 2b. Hence, as expected, at potentials lower than the inflection point potential (<0.35 V_{RHE} for 5 mV s⁻¹ and <0.20 V_{RHE} for 10 mV s⁻¹), the calculated Cu coverages exceed that of a monolayer, as shown in Fig. 3b.

At an even lower scan rate of 1 mV s⁻¹, the inflection point potential prior to Cu bulk deposition moves to a slightly more positive potential of ~0.40 V_{RHE} (marked by the red dashed arrow in Fig. 4a). The approximate Cu coverage reached at ~0.40 V_{RHE} (see gray area in Fig. 4a) and determined by a subsequent Cu stripping voltammetry at 1 mV s⁻¹ amounts to ~0.93 monolayers. Since the Cu stripping currents increase with increasing stripping scan rates and since the Cu stripping process is a rather fast process,³⁶ a better accuracy of the background corrected Cu stripping charge is expected for higher stripping scan rates. The dependency of the Cu stripping charge as a function of the stripping scan rate after Cu deposition in a preceding cathodic scan at 1 mV s⁻¹ (both in 0.1 M HClO₄ with 1 mM Cu²⁺) is depicted in Fig. 4b, showing that the Cu coverage when determined at 1–500 mV s⁻¹ ranges between ~0.93 and ~1.05 ML. In combination with Fig. 4a, these data suggest that the thermodynamic potential for a full Cu_{UPD} monolayer is near 0.40 V_{RHE}. Furthermore, since the Cu stripping kinetics are clearly

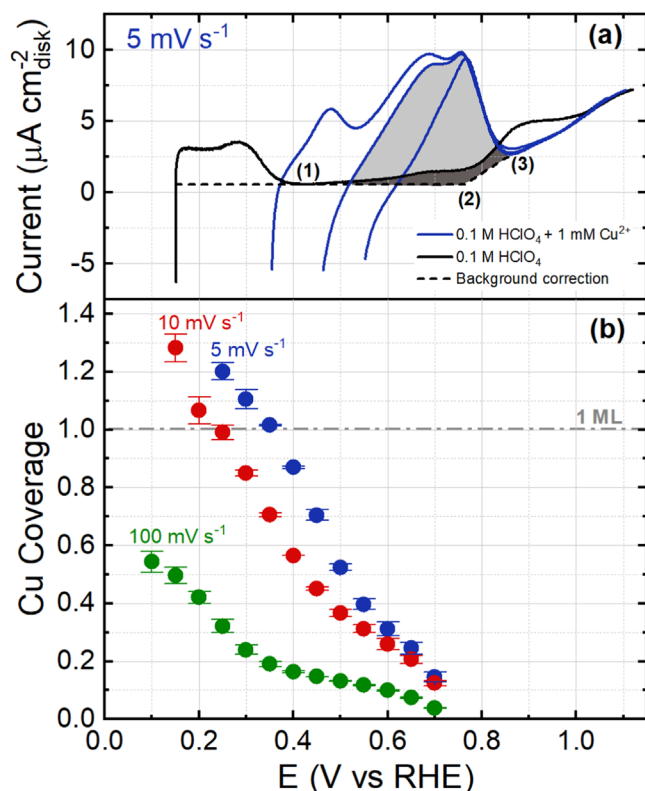


Figure 3. (a) Selection of the positive-going scans at 5 mV s⁻¹ (from Fig. 2a) for a Pt disk in 0.1 M HClO₄ with 1 mM Cu²⁺ at 400 rpm, recorded for negative potential limits of 0.35, 0.45, and 0.55 V_{RHE} (blue lines); the Pt disk CV in the Cu²⁺-free electrolyte is given as reference (black line) and the dashed black lines represent the here used approximation of the background charge (see text). (b) Cu coverage of a Pt disk estimated by the here adopted integration procedure (area between the Cu stripping scans and the black dashed lines) as a function of the cathodic potential limit and the CV scan rate, based on the data shown in Fig. 2 (0.1 M HClO₄ with 1 mM Cu²⁺ at 400 rpm under Ar purge).

fast enough to allow for a quantification of the Cu coverage at high stripping scan rates, we will be able to later on utilize this to quantify the Cu coverage in the presence of H₂ containing gas (see next section) without significant interference from the charge produced by the simultaneously occurring oxidation of dissolved hydrogen.

H₂ gas promoted Cu_{UPD} on a Pt disk.—In the following, we will examine the Cu deposition process driven by the equilibration of the initially air saturated Cu²⁺-containing electrolyte with either H₂ or with H₂/Ar gas mixtures. Owing to the high activity of platinum for the H₂ oxidation/evolution reaction (HOR/HER), the open circuit potential of a Pt electrode will shift towards the HOR/HER equilibrium potential (corresponding to 0 V vs RHE), which means that in this case the potential of the Pt electrode is lowered by the exposure to H₂ containing gas rather than by externally applying a negative potential (as was done, e.g., in the above described cathodic copper deposition CV scans). In either case, lowering the Pt potential into the potential region where UPD copper is being formed on Pt should lead to the formation of a Cu_{UPD} layer. A H₂ gas promoted Cu deposition approach was taken previously by Taufany et al.,³³ who deposited copper on palladium nanoparticles, and who stated that the Cu deposition process is driven either by the reaction of Cu²⁺ ions with adsorbed UPD hydrogen or by the redox reaction between Cu²⁺ and H₂ gas at the Pd surface; which of these two mechanisms is the more likely will be discussed later.

The open circuit potential of a Pt disk working electrode (rotated at 1600 rpm) upon purging the initially air saturated 0.1 M HClO₄ electrolyte with 100% H₂ is shown in Fig. 5a. In the absence of Cu²⁺

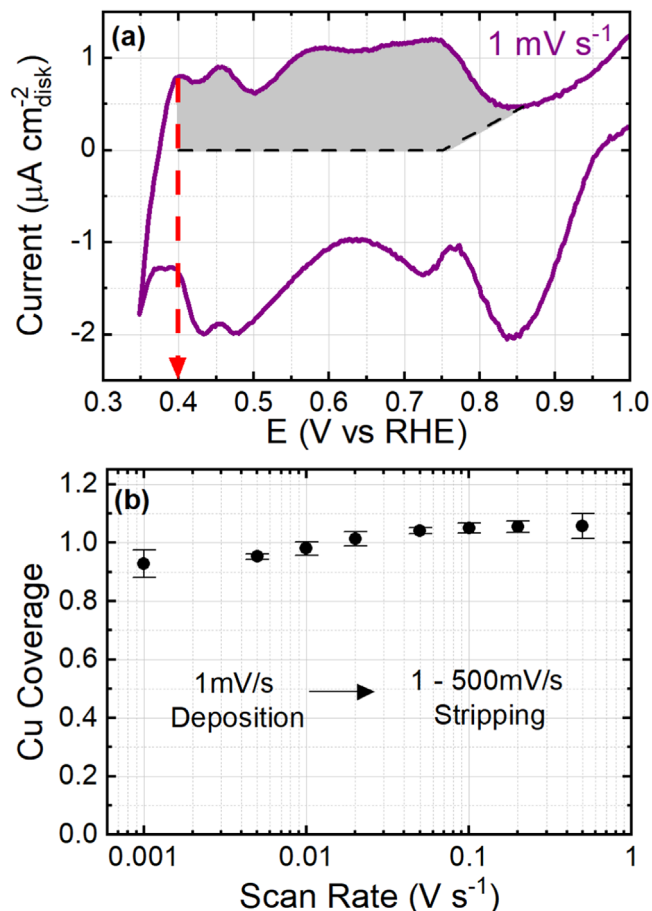


Figure 4. (a) Cu deposition scan from 1.0 V_{RHE} to 0.35 V_{RHE} and subsequent stripping scan (both at 1 mV s^{-1}) on a Pt disk in 0.1 M HClO_4 with 1 mM Cu^{2+} at 400 rpm under Ar purge. The approximate potential at which the Cu_{UPD} layer formation is completed is indicated by the dashed red arrow, marking the inflection point in the cathodic scan prior Cu bulk deposition. The Cu deposition charge is estimated to correspond to the gray marked area, using the background correction outlined in Fig. 3a. (b) Cu coverage (θ_{Cu}) on a Pt disk electrode as a function of the scan rate of the Cu stripping sweep, for the Cu deposition being carried out in a cathodic scan at 1 mV s^{-1} to 0.35 V_{RHE} in 0.1 M HClO_4 with 1 mM Cu^{2+} at 400 rpm under Ar purge.

ions, the potential rapidly drops towards 0 V_{RHE} , reaching +1 mV vs our RHE reference electrode after several minutes (black line). This is of course expected, as it is known that platinum in H_2 saturated acidic electrolytes readily establishes the HOR/HER equilibrium potential due to its high HOR/HER activity (the 1 mV deviation between our static RHE reference electrode and the Pt disk potential under 100% H_2 is within the absolute error of our RHE reference electrode). When 1 mM Cu^{2+} ions are present in the electrolyte, the OCP drop upon purging the initially air saturated electrolyte with 100% H_2 (red line, Fig. 5a) is equally rapid as that in the Cu^{2+} -free electrolyte, also reaching $\sim 0 V_{\text{RHE}}$ in short time. However, after several minutes, the OCP gradually increases, reaching a steady-state value of $\sim 0.28\text{--}0.29 V_{\text{RHE}}$. At this point, Cu bulk deposition was clearly visible on the surface of the electrode by the appearance of an orange film covering the Pt disk, suggesting that, similarly to an electrochemical Cu deposition potential step from $\sim 1 V_{\text{RHE}}$ to $\sim 0 V_{\text{RHE}}$, the rapid change of the Pt electrode's OCP into the HOR/HER equilibrium potential resulted in the formation of a multi-layer Cu deposit on the surface of the Pt electrode. Hence, the observed OCP of $\sim 0.28\text{--}0.29 V_{\text{RHE}}$ closely represents the Cu^{2+}/Cu equilibrium potential for a bulk Cu electrode. The experimental value of the latter is determined by monitoring the OCP of a metallic Cu disk electrode immersed into the same 0.1 M HClO_4 electrolyte with 1 mM Cu^{2+} , showing an OCP of $\sim 0.30 V_{\text{RHE}}$ that is not affected by purging

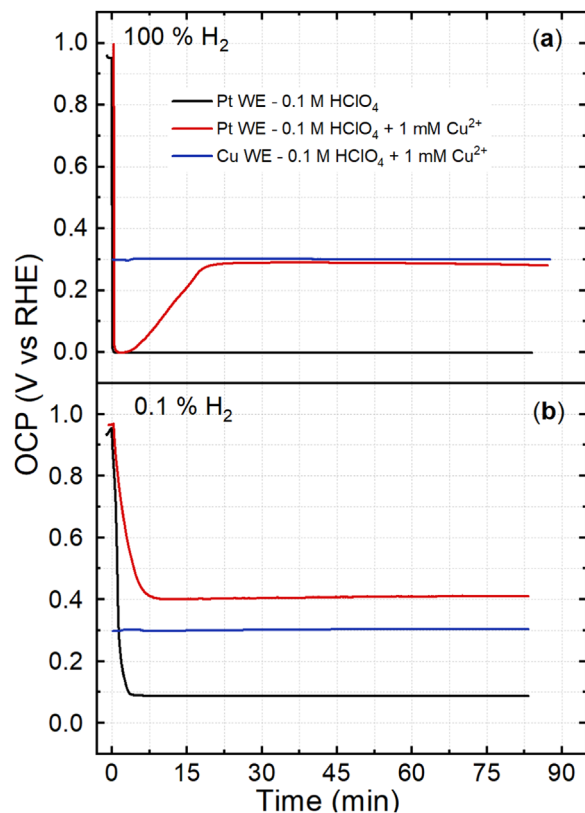


Figure 5. OCP transients obtained for a Pt disk working electrode (WE) immersed in 0.1 M HClO_4 without Cu^{2+} (black) or with 1 mM Cu^{2+} (red) upon purging the initially air saturated electrolyte at $t \geq 0$ with (a) 100% H_2 or with (b) 0.1% H_2/Ar . The blue lines depict an analogous experiment conducted with a Cu disk WE in the same Cu^{2+} -containing electrolyte. To avoid possible Cu^{2+} mass transport limitations, the disk working electrodes were rotated at 1600 rpm.

the initially air saturated electrolyte with 100% H_2 (blue line), which can be explained by extremely low activity of copper towards the HER/HOR.³⁹ This measured value of $\sim 0.30 V_{\text{RHE}}$ for the Cu disk in 1 mM Cu^{2+} -containing electrolyte can also be compared to the Cu^{2+}/Cu equilibrium potential calculated from the Nernst equation:

$$E_{\text{Cu}/\text{Cu}^{2+}} = E_{\text{Cu}/\text{Cu}^{2+}}^0 + \frac{RT}{2F} \ln[a_{\text{Cu}^{2+}}] \quad [2]$$

Here, $E_{\text{Cu}/\text{Cu}^{2+}}^0$ is the standard Cu^{2+}/Cu potential of $\sim 0.34 \text{ V}$ vs the standard hydrogen electrode (SHE) potential,⁴³ R is the ideal gas constant ($8.315 \text{ J mol}^{-1} \text{ K}^{-1}$), F is the Faraday constant ($96485 \text{ A s mol}^{-1}$), and $a_{\text{Cu}^{2+}}$ is the copper activity of the 1 mM Cu^{2+} -containing electrolyte that can be approximated by $a_{\text{Cu}^{2+}} \approx 1 \text{ mM}/1 \text{ M} = 10^{-3}$. Thus, the Cu^{2+}/Cu equilibrium potential in this electrolyte is $\sim 0.25 \text{ V}$ vs SHE. Since the RHE reference electrode is based on 0.1 M HClO_4 electrolyte with an approximate proton activity of $a_{\text{H}^+} \approx 0.1$ that is saturated with H_2 gas at 1 bar, the here measured RHE potential is $\sim 0.06 \text{ V}$ negative of 0 V vs SHE, as determined again by the Nernst equation:

$$E_{\text{H}_2/\text{H}^+} = E_{\text{H}_2/\text{H}^+}^0 + \frac{RT}{2F} \ln \left[\frac{(a_{\text{H}^+})^2}{\left(\frac{P_{\text{H}_2}}{1 \text{ bar}} \right)} \right] \quad [3]$$

Based on this, the predicted Cu^{2+}/Cu equilibrium potential in 1 mM Cu^{2+} in 0.1 M HClO_4 is $\sim 0.31 \text{ V}$ vs the here used RHE reference electrode potential, which is in reasonably good agreement with the $\sim 0.30 V_{\text{RHE}}$ measured for the Cu disk electrode.

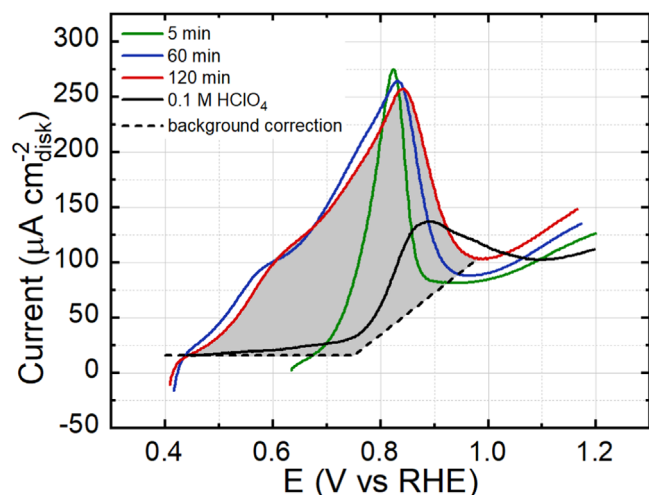


Figure 6. Copper stripping CVs at 100 mV s^{-1} obtained after the H_2 promoted deposition of Cu on the Pt disk electrode in $0.1 \text{ M HClO}_4 + 1 \text{ mM Cu}^{2+}$ after different purge times with $0.1\% \text{ H}_2/\text{Ar}$, namely 5 min (green), 60 min (blue), and 120 min (red). The black line shows the “stripping” CV of the Pt disk after ~ 10 min of $0.1\% \text{ H}_2/\text{Ar}$ purge in the 0.1 M HClO_4 base electrolyte without Cu^{2+} . The Pt disk was rotated at 1600 rpm during Cu deposition, while the stripping CVs were conducted at 0 rpm but still maintaining the $0.1\% \text{ H}_2/\text{Ar}$ purge. The Cu coverage was determined from the charge under the Cu stripping CV minus the background correction (black dashed line), as illustrated exemplarily for a purge time of 120 min (red line) by the gray marked area.

As expected from the observed surface change on the Pt electrode while recording the transient shown in Fig. 5a, the Cu^{2+}/Cu equilibrium potential measured for the Cu disk is within ~ 0.01 – 0.02 V of the steady-state OCP obtained for the Pt disk electrode. This confirms once more that the H_2 gas promoted copper deposition on the Pt disk resulted in a multi-layer/bulk copper deposit. The somewhat lower OCP of the latter furthermore suggests that a small fraction of platinum sites must remain in contact with the electrolyte, i.e., that a perfect coverage of the Pt disk with copper has not been achieved. The formation of a Cu multi-layer/bulk copper deposit on the Pt disk rather than of a Cu_{UPD} monolayer is further supported by the fact that the equilibrium potential of the latter would be have to be $\sim 0.40 \text{ V}_{\text{RHE}}$, as was revealed by the Cu deposition/stripping voltammetry at 1 mV s^{-1} in Fig. 4a.

In order to investigate if the formation of a Cu_{UPD} monolayer on the Pt disk can be obtained by H_2 gas promoted Cu deposition at OCP conditions, the effect of lowering the hydrogen concentration was evaluated. The OCP was again monitored over the course of purging an initially air saturated electrolyte with a mixture of 0.1% of H_2/Ar . In the pure 0.1 M HClO_4 electrolyte, the OCP of the Pt electrode decreased at an approximate rate of 4 mV s^{-1} , requiring ~ 3 min to reach a constant OCP of $\sim 0.09 \text{ V}_{\text{RHE}}$ (black line, Fig. 5b), much slower than in the case where $100\% \text{ H}_2$ was used (black line, Fig. 5a). The higher steady-state OCP value is consistent with the predicted $\sim 0.09 \text{ V}$ more positive HOR/HER equilibrium potential with respect to our RHE reference electrode, due to the 10^3 times lower H_2 partial pressure in this case (acc. to Eq. 3, with $\sim 1 \text{ mbar}$ for $0.1\% \text{ H}_2/\text{Ar}$ vs $\sim 1 \text{ bar}$ for $100\% \text{ H}_2$). Furthermore, in the 0.1 M HClO_4 electrolyte with 1 mM Cu^{2+} , the OCP decreased at a much slower rate when using $0.1\% \text{ H}_2/\text{Ar}$ (at $\sim 1 \text{ mV s}^{-1}$), gradually reaching a steady-state value of $\sim 0.40 \text{ V}_{\text{RHE}}$ after ~ 8 min of initiation of the $0.1\% \text{ H}_2/\text{Ar}$ purge (red line in Fig. 5b). Remarkably, in this case the OCP did not initially dip to potentials near the HER/HOR equilibrium potential as was observed when using $100\% \text{ H}_2$, but gradually decreased to the potential that is expected to be at/near the equilibrium potential of a full Cu_{UPD} monolayer on the Pt disk (at $\sim 0.40 \text{ V}_{\text{RHE}}$), which is well above the Cu^{2+}/Cu potential of $\sim 0.30 \text{ V}_{\text{RHE}}$ for a bulk Cu disk electrode (blue

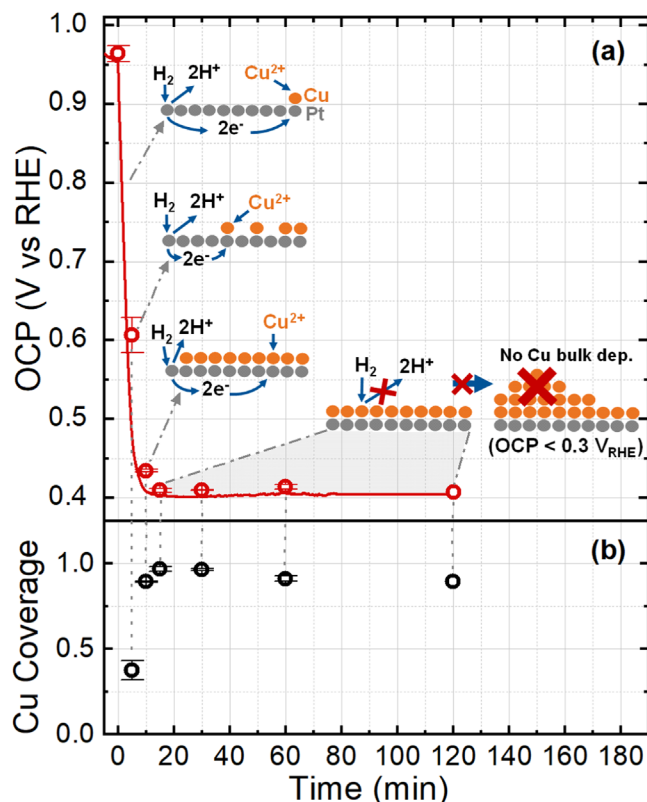


Figure 7. (a) OCP transients obtained for a Pt disk in 0.1 M HClO_4 with 1 mM Cu^{2+} upon purging the initially air saturated electrolyte with $0.1\% \text{ H}_2/\text{Ar}$ while rotating the Pt disk at 1600 rpm . The left-most red circle denotes the OCP in the initially air saturated electrolyte, while the other red circles denote the OCP under the $0.1\% \text{ H}_2/\text{Ar}$ purge at the different times at which Cu stripping CVs were initiated (conducted at 0 rpm but maintaining the $0.1\% \text{ H}_2/\text{Ar}$ purge); the red line exemplarily shows the OCP transient for one experiment with a deposition time of 120 min (b) Cu coverage as a function of time determined from the Cu stripping CV analysis following the procedure outlined in Fig. 6. The error bars represent the standard deviation for two repeated experiments. The sketches in (a) represent the here deduced copper deposition mechanisms at the different OCP values during the experiment; Cu bulk deposition is prevented by the inactivity of the Cu_{UPD} layer towards the HOR.

line in Fig. 5b). Therefore, the slow OCP decrease of the Pt disk electrode when purging the initially air saturated electrolyte with dilute H_2 gas ($0.1\% \text{ H}_2/\text{Ar}$) seems to result in the formation of a Cu_{UPD} layer as in the case of a slow cathodic CV scan (see Fig. 4a). The fact that the observed steady-state OCP in the electrolyte saturated with $0.1\% \text{ H}_2/\text{Ar}$ remains at/near the value expected for a Cu_{UPD} monolayer furthermore suggests a full coverage of all Pt sites, as Pt sites exposed to the electrolyte would be expected to bias the OCP towards the Cu multi-layer/bulk deposition potential ($\sim 0.30 \text{ V}_{\text{RHE}}$). In summary, these data suggest that a self-limiting Cu_{UPD} monolayer can be produced on a Pt disk electrode at OCP by saturating the $0.1 \text{ M HClO}_4 + 1 \text{ mM Cu}^{2+}$ electrolyte with a H_2 containing gas that is sufficiently dilute to allow a slow decrease of the OCP from ~ 0.90 – $0.95 \text{ V}_{\text{RHE}}$ in the air saturated electrolyte to the equilibrium potential of a full Cu_{UPD} monolayer on the Pt disk (at $\sim 0.40 \text{ V}_{\text{RHE}}$).

This can be confirmed by evaluating the Cu coverage after different purging times with $0.1\% \text{ H}_2/\text{Ar}$, expecting that a full Cu_{UPD} coverage is obtained once the steady-state OCP of $\sim 0.40 \text{ V}_{\text{RHE}}$ is reached. For this, copper stripping CVs were recorded after different purging times in the same cell where the deposition took place, while maintaining the $0.1\% \text{ H}_2/\text{Ar}$ purge during the copper stripping CV in order to reduce the risk of Cu dissolution that would occur if O_2 were to diffuse into the electrolyte solution.⁴⁴ At the chosen copper

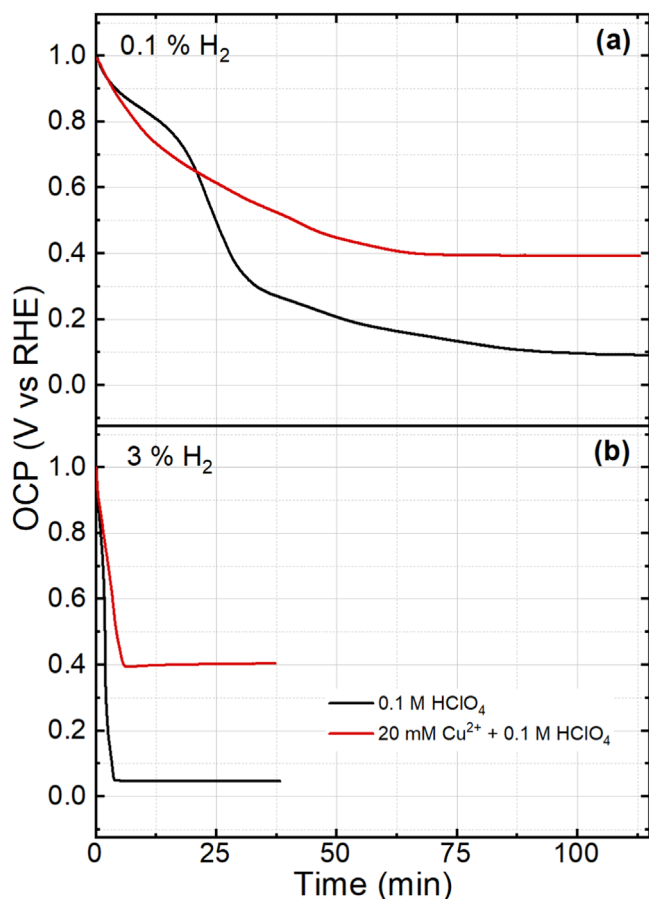


Figure 8. OCP transients obtained for a Pt/C thin-film RDE (with a Pt loading of $33 \mu\text{g}_{\text{Pt}} \text{cm}^{-2}_{\text{disk}}$) immersed in 0.1 M HClO_4 without Cu^{2+} (black) or with 20 mM Cu^{2+} (red) upon purging the initially air saturated electrolyte at $t \geq 0$ with (a) 0.1% H_2/Ar or with (b) 3% H_2/Ar . To avoid possible Cu^{2+} mass transport limitations, the thin-film RDE working electrodes were rotated at 1600 rpm.

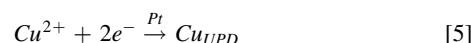
stripping CV scan rate of 100 mV s^{-1} , the charge contribution from the oxidation of dissolved H_2 at such low H_2 concentrations is negligible, while it allows for a precise quantification of the copper coverage as shown in Fig. 3. The solid black line in Fig. 6 depicts the anodic CV scan obtained in the 0.1 M HClO_4 base electrolyte under the 0.1% H_2/Ar purge at 100 mV s^{-1} , demonstrating an as expected negligible contribution from H_2 oxidation. The copper stripping CVs obtained after 5, 60, and 120 min of the 0.1% H_2/Ar purge are presented as an example in Fig. 6. Figure 6 furthermore illustrates exemplarily for the 120 min purge time the background correction (black dashed lines in Fig. 6) that was used to quantify the copper stripping charge (gray area), following the procedure outlined in Fig. 3a. The small differences in the curves obtained after 60 and 120 min which have both exhibited the same steady-state OCP of $\sim 0.40 \text{ V}_{\text{RHE}}$ may suggest a minor restructuring of the Cu ad-atoms towards a more stable configuration with time, which might lead to the observed slightly higher potentials for the complete stripping of the Cu UPD layer.

The thus determined Cu coverages after different deposition times under 0.1% H_2/Ar purge in 0.1 M $\text{HClO}_4 + 1 \text{ mM Cu}^{2+}$ (i.e., for a series of experiments analogous to those in Fig. 5b) are shown in Fig. 7b (black symbols), whereby Fig. 7a depicts the simultaneously recorded OCP values (red symbols); the error bars represent the standard deviation for two repeat experiments (the red line exemplarily shows the OCP transient for one experiment with a deposition time of 120 min). The average OCP of $\sim 0.96 \text{ V}_{\text{RHE}}$ in the initially air saturated electrolyte gradually decreases upon purging the electrolyte with 0.1% H_2/Ar (red symbols), accompanied by an

increase in the copper coverage (black symbols in Fig. 7b). Within 5 min of purge time, the OCP decreases to $\sim 0.61 \text{ V}_{\text{RHE}}$ (second red circle from the left), i.e., decreasing at an average rate of $\sim 1 \text{ mV s}^{-1}$, accompanied by the formation of a Cu_{UPD} layer with a coverage of ~ 0.37 (first black circle from the left). Here, the H_2 oxidation reaction catalyzed by platinum induces a negative shift of the OCP at a very low rate of $\sim 1 \text{ mV s}^{-1}$ that results from the low H_2 concentration in the electrolyte in equilibrium with 0.1% H_2/Ar :

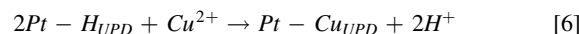


As the potential decreases below $\sim 0.8 \text{ V}_{\text{RHE}}$, the underpotential deposition of copper via the reduction of Cu^{2+} ions in the electrolyte becomes thermodynamically favorable (see Fig. 2), as depicted in the left-most sketch in Fig. 7a:



As in this case it is irrelevant whether the OCP is lowered by the oxidation of H_2 according to Eq. 4 or by externally controlling the potential of the platinum electrode in a CV experiment (see Fig. 2), the Cu_{UPD} coverage at a given OCP value should be independent of whether the Cu_{UPD} formation is induced by the exposure to H_2 containing gas or by a cathodic CV scan, as long as the final deposition potential and the effective rate of OCP decrease are comparable. This expectation is indeed reasonably closely matched: for a cathodic CV scan of 5 mV s^{-1} (blue symbols in Fig. 3b), a Cu coverage of ~ 0.31 is obtained at $0.60 \text{ V}_{\text{RHE}}$, while a Cu coverage of ~ 0.37 is obtained at an OCP of $\sim 0.61 \text{ V}_{\text{RHE}}$ in the H_2 promoted Cu deposition with 0.1% H_2/Ar , where the cathodic OCP shift is $\sim 1 \text{ mV s}^{-1}$ (Fig. 7).

An alternative deposition mechanism that has been suggested is that Cu_{UPD} formation in the presence of H_2 could be due to the reaction of UPD hydrogen on Pt according to:^{22,23,33}



However, for the H_2 promoted Cu deposition shown in Fig. 7, this mechanism can clearly be excluded, as potentials $> 0.40 \text{ V}_{\text{RHE}}$ are positive of the H_{UPD} region of polycrystalline platinum (see black line in Fig. 2a), which means that the H_{UPD} coverage at the OCP of $\sim 0.61 \text{ V}_{\text{RHE}}$ is essentially zero, while a Cu coverage of already ~ 0.37 has been formed at this point (see Fig. 7).

After purging the electrolyte with 0.1% H_2/Ar for 10 min, the OCP decreases to $\sim 0.43 \text{ V}_{\text{RHE}}$ (third red circle in Fig. 7a) and the Cu coverage increases to ~ 0.89 (second black circle in Fig. 7b), indicating a nearly complete Cu_{UPD} monolayer. After 15 min, the OCP reaches a steady-state value of $\sim 0.40 \text{ V}_{\text{RHE}}$ and an essentially full Cu_{UPD} monolayer is deduced from the Cu stripping voltammogram within the accuracy of this measurement. While the bulk deposition of Cu in the presence of H_2 would be thermodynamically favored, the Cu_{UPD} layer is apparently inactive for the H_2 oxidation reaction (HOR), so that the OCP cannot be lowered anymore by the oxidation of H_2 on the Pt electrode (Eq. 4) to the lower potential of $\sim 0.30 \text{ V}_{\text{RHE}}$ that would be required for Cu bulk deposition. This leads to a stabilization of the Cu_{UPD} monolayer or, in other words, to the formation of a self-limiting Cu_{UPD} monolayer by the H_2 promoted copper deposition on platinum. This, however, requires that the H_2 containing gas is sufficiently dilute to result in a slow decrease of the OCP, since otherwise the rapid H_2 oxidation will lower the Pt electrode potential to the HOR/HER equilibrium potential that is negative of the Cu bulk deposition potential and thus lead to Cu bulk deposition (see Fig. 5a).

H_2 gas promoted Cu_{UPD} on a Pt/C thin-film RDE.— Considering that the chemical deposition method described above could be used as a first step in the preparation of Cu_{UPD} decorated catalyst precursor materials, it is of great interest to determine if the self-limiting H_2 promoted Cu_{UPD} monolayer deposition process can

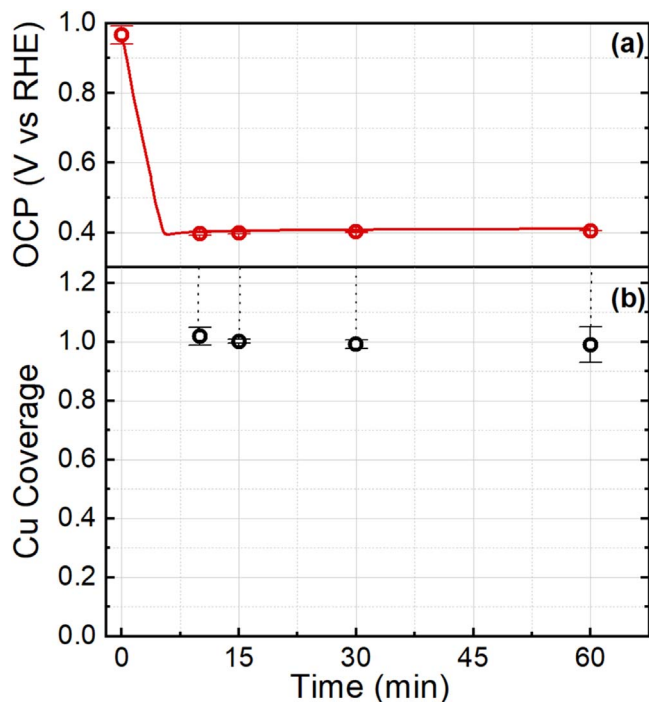


Figure 9. (a) OCP transients obtained for a Pt/C thin-film electrode in 0.1 M HClO₄ with 20 mM Cu²⁺ upon purging the initially air saturated electrolyte with 3% H₂/Ar while rotating the Pt/C thin-film disk electrode at 1600 rpm. The left-most red circle denotes the OCP in the initially air saturated electrolyte, while the other red circles denote the OCP under the 3% H₂/Ar purge at the different times at which Cu stripping CVs were initiated (conducted at 0 rpm but maintaining the 3% H₂/Ar purge); the red line exemplarily shows the OCP transient for one experiment with a deposition time of 60 min (b) Cu coverage as a function of time determined from the Cu stripping CV analysis following the procedure outlined in Fig. 6. The error bars represent the standard deviation for two repeated experiments.

be transferred to Pt nanoparticles supported on carbon, i.e., to a Pt/C catalyst. Therefore, thin-film RDE working electrodes with a Pt/C catalyst attached to a glassy carbon RDE substrate were prepared using a commercial 46.1 wt% Pt/C catalyst and Nafion®. In contrast to the experiments with the polycrystalline Pt disk electrodes, the Cu²⁺ concentration in the electrolyte was increased to 20 mM in order to avoid Cu²⁺ transport limitations to the platinum electrode that has a ~15-fold higher roughness factor for the Pt/C thin-film RDE compared to the polycrystalline Pt disk. The impact of Cu²⁺ transport limitations for the Pt/C thin-film RDE was observed in cathodic Cu deposition CVs in 0.1 M HClO₄ with 1 mM Cu²⁺ at a scan rate of 20 mV s⁻¹ (data not shown). On the other hand, for the higher Cu²⁺ concentration of 20 mM, the cathodic Cu deposition CVs followed the trends shown in Fig. 3, except that the Cu²⁺/Cu bulk deposition potential now shifted from ~0.31 to ~0.35 V_{RHE}, as predicted by Eq. 2 for the 20-fold higher Cu²⁺ concentration.

The OCP transient of the Pt/C thin-film RDE rotating at 1600 rpm was recorded while purging the initially air saturated electrolyte with 0.1% H₂/Ar, analogous to the experiments shown in Fig. 5b. The black line in Fig. 8a shows the OCP vs time in the Cu²⁺-free 0.1 M HClO₄ base electrolyte, reaching the HOR/HER equilibrium potential of ~0.09 V_{RHE} vs our RHE reference electrode as in the case of the polycrystalline Pt disk electrode (see Fig. 5b), except that reaching this final value took ~20 times longer time. Combined with the observation that the time to reach the HOR/HER equilibrium potential was much shorter also for Pt/C thin-film electrodes with a lower Pt loading (data not shown), this suggests that the long OCP transition time is likely related to H₂ transport limitations. The plausibility of this hypothesis can be verified by comparing the estimated H₂ transport rate with the charge required

to polarize the electrode to the HOR/HER equilibrium potential when starting at an OCP of ~0.98 ± 0.02 V_{RHE} (i.e., at t = 0 in Fig. 8a). The limiting HOR current density in 0.1 M HClO₄ at 1600 rpm and room temperature is reported to be ~2.5 mA cm⁻²_{disk} for an electrolyte purged with pure H₂;⁴⁵ for the here used purge with 0.1% H₂/Ar, the limiting HOR current would thus be ~2.5 μA cm⁻²_{disk} (assuming Henry's Law). Lowering the OCP of the Pt/C catalyst from initially ~0.98 V_{RHE} (i.e., from the Pt-OH region) to the HOR/HER equilibrium potential (i.e., to the region with a full H_{UPD} coverage) requires that the reduction charge under the Pt/C CV must be provided by the oxidation of H₂ (Eq. 2). For the here used catalyst, this reduction charge was determined from a CV between these two potential limits and amounts to ~545 μC cm⁻²_{Pt} or, considering the roughness factor of ~18 cm²_{Pt} cm⁻²_{disk}, to ~9800 μC cm⁻²_{disk}. Thus, the H₂ transport limited time to shift the OCP from ~0.98 V_{RHE} to the HOR/HER equilibrium potential can be approximated by dividing the required charge (~9800 μC cm⁻²_{disk}) by the limiting HOR current density (~2.5 μA cm⁻²_{disk}), equating to ~3920 s or ~65 min. As the estimated H₂ transport limited time of ~65 min is reasonably close to the time for the OCP to reach the HOR/HER equilibrium potential, the long transition time must be due to H₂ transport limitations and thus should be inversely proportional to the H₂ concentration of the purge gas (this will, indeed, be confirmed in the next paragraph). Conducting the same experiment in 0.1 M HClO₄ with 20 mM Cu²⁺ (red line in Fig. 8a) reveals an equally slow OCP drop to a steady-state potential of ~0.40 V_{RHE}, a potential which indicates the formation of a full Cu_{UPD} monolayer, as discussed in the context of Fig. 5b. Also here, the slow OCP drop prevents the formation of bulk Cu deposition. The OCP transition time in the presence and absence of Cu²⁺ is roughly the same, as would be expected if the transition time is controlled by the H₂ transport rate, since the Cu_{UPD} monolayer charge is the same as the H_{UPD} charge.

Under this premise, the OCP transition time should be reduced, if the H₂ transport rate is increased, which can be done easily by increasing the H₂ concentration in the purge gas. Thus, by increasing the H₂ concentration from 0.1% H₂/Ar to 3% H₂/Ar, a ~30-fold faster OCP transition time would be expected. As shown in Fig. 8b, this is indeed the case. In pure 0.1 M HClO₄ (black line), the OCP reaches the HOR/HER equilibrium potential of ~45 mV_{RHE} (consistent with Eq. 3, based on ~30 mbar for 3% H₂/Ar vs ~1 bar for 100% H₂) within ~3.5 min, which is indeed ~30 times faster than for the experiment with 0.1% H₂/Ar (black line in Fig. 8a). This corresponds to an average decrease of the OCP of ~4 mV s⁻¹, which should still be slow enough to allow for the formation of a Cu_{UPD} monolayer without Cu bulk deposition. This is confirmed by the H₂ promoted Cu deposition with 3% H₂/Ar in the 0.1 M HClO₄ + 20 mM Cu²⁺ electrolyte (red line in Fig. 8b), where the steady-state OCP of ~0.40 V_{RHE} is reached within ~6 min (corresponding to ~1.5 mV s⁻¹), suggesting the self-limiting formation of a Cu_{UPD} monolayer.

The formation of a self-limiting Cu_{UPD} monolayer on the platinum surface of the Pt/C catalyst is confirmed by an examination of the Cu coverage as a function of time, determined by copper stripping CVs, following the procedure outlined in Figs. 6 and 7 for the polycrystalline platinum disk. Here, the Cu coverage shown in Fig. 9 could not be determined over the course of the initial OCP drop (as done in Fig. 7), since the transition time was too short. However, for the steady-state OCP potential of ~0.40 V_{RHE}, the Cu coverage corresponds to a full monolayer within the error of measurement (see Fig. 9b), indicating that self-limiting Cu_{UPD} monolayer coverages can also be achieved on the platinum surface of a Pt/C catalyst.

In summary, by increasing the H₂ concentration in the purge gas, the rate of the Cu deposition process can be increased, whereby the H₂ concentration must be kept low enough to still limit the rate of the OCP drop at a sufficiently low value to avoid Cu bulk deposition. Based on the Cu deposition/stripping CVs shown in Fig. 2, this

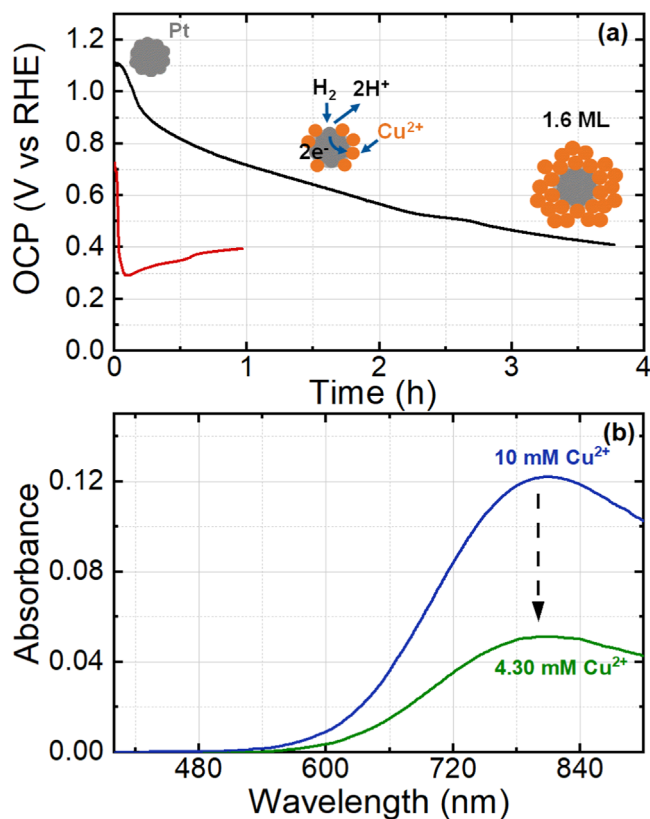


Figure 10. (a) OCP transients of the Pt-wire sensing electrode measured in the reaction cell (see Fig. 1a) upon purging the initially air saturated electrolyte (0.1 M HClO₄ + 10 mM Cu²⁺) with 5% H₂/Ar. Red line: Pt-wire OCP in the absence of the Pt/C catalyst; black line: Pt-wire OCP in the presence of 0.5 g of a 46.1 wt% Pt/C catalyst dispersed in 80 ml of electrolyte. (b) UV-Vis spectra of the as-prepared electrolyte with 10 mM Cu²⁺ in 0.1 M HClO₄ (blue) and of the filtrated electrolyte once the copper deposition process has progressed until the Pt-wire sensing electrode OCP has reached an OCP of 0.40 V_{RHE} (green). The sketches in (a) represent a simplified depiction of the copper deposition mechanisms at the different OCP values during the experiment.

limiting rate is estimated to be near 10 mV s⁻¹, since at much higher scan rates, the Cu_{UPD} monolayer will not be completed prior to Cu bulk deposition (as discussed in the context of Figs. 2 and 3b).

H₂ promoted deposition of UPD Cu on an electrolyte-dispersed Pt/C catalyst.—Based on the knowledge obtained from the Pt disk and Pt/C thin-film RDE experiments, the H₂ promoted Cu deposition was implemented to prepare 0.5 g of a 46.1 wt% Pt/C catalyst with a Cu_{UPD} coverage close to a monolayer (Cu_{UPD}Pt/C). The Cu_{UPD}Pt/C material was prepared in the reaction cell shown in Fig. 1, which was designed to allow for the H₂ promoted Cu deposition as well as for the collection, washing, and drying of the Cu_{UPD}Pt/C material under a continuous purge with a H₂ containing gas in order to prevent contact with ambient air. For this, 0.5 g Pt/C were dispersed in 80 ml of a 0.1 M HClO₄ electrolyte with 10 mM Cu²⁺, whereby the total moles of Cu²⁺ in the reaction cell was ~3-fold higher than the moles of Cu²⁺ required to form a Cu_{UPD} monolayer on the Pt surface exposed by the catalyst (based on the measured Pt dispersion of ~55 m²_{Pt} g⁻¹_{Pt} and a specific charge of 210 μC cm⁻²_{Pt}, 0.5 g of the 46.1 wt% Pt/C catalyst expose ~0.26 mmol Pt surface atoms). Compared to the above discussed Pt/C thin-film RDE experiments with only ~6.5 μg_{Pt} in the disk, the total amount of Pt in the reaction cell of ~230 μg_{Pt} is much larger, so that we increased the H₂ concentration in the purge gas to 5% H₂/Ar in order to minimize the reaction time (for safety reasons, 5% was the maximum H₂ concentration we could use with the reaction cell).

As shown by the above thin-film RDE experiments, the progress of the H₂ promoted Cu deposition on a Pt/C catalyst can be monitored quite effectively by the OCP. This, however, cannot be measured directly for Pt/C particles dispersed in the electrolyte, so that a Pt-wire sensing electrode was immersed into the electrolyte, whose OCP was measured vs a RHE reference electrode (see Fig. 1). The rationale as to why the OCP and the associated Cu coverage of the Pt-wire sensing electrode should closely represent that of the dispersed Pt/C particles is based on two assumptions: i) that the local H₂ mass transport to the dispersed Pt/C particles and to the Pt-wire sensing electrode should be similar; in which case, based on the above findings that the H₂ promoted Cu deposition process is largely limited by the local H₂ mass transport rate, this would yield similar Cu coverages and thus similar OCP values; ii) that through the intermittent contact of the Pt-wire with the dispersed Pt/C catalyst particles, their OCP would be expected to equilibrate. To validate this approach, we first measured the OCP response of the Pt-wire sensing electrode when purging the initially air saturated 0.1 M HClO₄ + 10 mM Cu²⁺ electrolyte with 5% H₂/Ar in the absence of dispersed Pt/C catalyst. The resulting OCP response is shown by the red line in Fig. 10a, where the OCP initially decreases within ~5 min into the Cu bulk deposition potential region of ~0.30 V_{RHE}, but then gradually increases to a steady-state value of ~0.40 V_{RHE}, indicating the formation of a Cu_{UPD} monolayer. This behavior is reminiscent to that observed in Fig. 5a (red line), except that the initial excursion to potentials negative of the Cu_{UPD} monolayer potential is not as pronounced here, due to the slower OCP transient.

In contrast to the OCP response of the Pt-wire sensing electrode in the absence of the Pt/C catalyst, its OCP response changes significantly when recorded in the presence of the Pt/C catalyst dispersed in the electrolyte (black curve, Fig. 10a), where the OCP of the Pt-wire sensing electrode now decreases very slowly with an approximate rate of 0.05 mV s⁻¹. Quite clearly, in the presence of the very large platinum surface area exposed by the dispersed Pt/C catalyst, much larger amounts of H₂ dissolved in the electrolyte are required for the HOR to provide the cathodic charge for the platinum oxide reduction and for the reduction of Cu²⁺ ions to form UPD copper, so that the Cu deposition process is again strongly H₂ mass transport limited, as in the case of the Pt/C thin-film RDE experiment with only 0.1% H₂/Ar (see Fig. 8a). As these H₂ mass transport limitations also affect the Cu deposition on the Pt-wire, its OCP also decreases very slowly and thus serves as an indirect measure of the progress of the Cu deposition process on the Pt nanoparticles of the Pt/C catalyst.

As shown in Fig. 10a, in the presence of the Pt/C catalyst, the OCP of the Pt-wire sensing electrode approached the Cu_{UPD} monolayer OCP of ~0.40 V_{RHE} over the course of ~4 h. However, preliminary deposition experiments with this setup with a Pt/C catalyst showed that the OCP of the Pt-wire SE continues to decrease below the value of 0.40 V_{RHE}, contrary to what was observed in the experiments with a Pt disk (Fig. 7) or a thin-film RDE (Fig. 9), as will also be discussed later in the context of Fig. 11. For this reason, the deposition experiment shown in Fig. 10a was interrupted once the Pt-wire SE OCP reached the potential of 0.40 V_{RHE} by turning the reaction cell upside down in order to separate the Cu_{UPD}Pt/C reaction product from the electrolyte that was subsequently removed by vacuum filtration (see Fig. 1b). To evaluate the amount of copper deposited on the thus obtained catalyst, two approaches were taken. The first approach was to determine the amount of copper in the retrieved Cu_{UPD}Pt/C material by elemental analysis, which resulted in a molar Pt:Cu ratio of 71:29. Another approach was to quantify the amount of copper consumed from the electrolyte by UV-vis analysis of the Cu²⁺ concentration in the filtrated electrolyte. The UV-vis spectra of the pristine electrolyte with 10 mM Cu²⁺ is shown in Fig. 10b (blue line) and compared to that of the filtrated electrolyte (green line), which based on our calibration curve corresponds to 4.30 mM Cu²⁺ (the molar extinction coefficient from our calibration of ε = 11.92 liter mol⁻¹ cm⁻¹ is in good agreement with values for similar

solutions⁴⁶). Based on the 80 ml of electrolyte that were used, this equates to a consumption of 0.46 mmol of Cu^{2+} . Since the 0.5 g of the 46.1 wt% Pt/C correspond to 0.23 g of Pt or 1.18 mmol of Pt, the thus obtained molar Pt:Cu ratio of the $\text{Cu}_{\text{UPD}}\text{Pt}/\text{C}$ material equates to 72:28, in good agreement with the elemental analysis.

Considering that copper is deposited onto the Pt nanoparticles, we can now estimate an equivalent copper coverage obtained in the experiment shown in Fig. 10. The specific Pt surface area of the Pt/C catalyst was determined to be $55 \text{ m}^2_{\text{Pt}} \text{ g}^{-1}_{\text{Pt}}$ (see Experimental section), which corresponds to an overall Pt surface area of 12.7 m^2 for the 0.23 g of Pt in the cell. Based on the here assumed $210 \mu\text{C cm}^{-2}_{\text{Pt}}$ and a 1-electron charge for H-UPD, this corresponds to 0.28 mmol of exposed Pt surface atoms. The estimated copper coverages for the deposited 0.46 mmol of copper would thus be equivalent to an average formation of ~ 1.6 monolayers. This deposition of a clearly more than 1 monolayer equivalent of copper in the experiment shown in Fig. 10, even though the reaction was stopped at the potential of $0.40 \text{ V}_{\text{RHE}}$ that in case of the Pt disk and the thin-film RDE experiments corresponded to a Cu_{UPD} monolayer, indicates that the H_2 promoted Cu deposition is not self-limiting in this case. Since the OCP drop was kept slow enough to avoid Cu bulk deposition and since the deposition reaction was interrupted at the established monolayer OCP of $0.40 \text{ V}_{\text{RHE}}$, this suggests that the reaction environment in this deposition configuration (see Fig. 1a) must be different to that in the Pt disk and thin-film RDE experiments, allowing for Cu multi-layer deposition.

To explore this hypothesis, a second deposition experiment was conducted to obtain some insight on what could be promoting the further deposition of Cu on the electrolyte-dispersed Pt/C catalyst. This experiment was performed with 0.5 g of a 20.0 wt% Pt/C catalyst with a dispersion of $\sim 76 \text{ m}^2_{\text{Pt}} \text{ g}^{-1}_{\text{Pt}}$ in order to slightly reduce the reaction time with the 5% H_2/Ar purge for the same amount of catalyst, since in this case the total moles of exposed Pt surface atoms in the reaction cell is only $\sim 0.17 \text{ mmol}$, i.e., ~ 1.7 -fold lower compared to the example shown in Fig. 10. At the same time, the molar ratio between the Cu^{2+} in the initial electrolyte solution and the moles of exposed Pt surface was kept the same as in the experiments with the 46.1 wt% Pt/C catalyst (~ 3 -fold excess) by using 110 ml of a 0.1 M HClO_4 electrolyte solution with 5 mM Cu^{2+} .

Similar to the experiment with the 46.1 wt% Pt/C catalyst (Fig. 10), the OCP of the Pt-wire sensing electrode immersed in the initially air saturated 0.1 M $\text{HClO}_4 + 5 \text{ mM Cu}^{2+}$ electrolyte solution with the 20.0 wt% Pt/C catalyst was monitored vs purging time with 5% H_2/Ar , as presented in Fig. 11b. At the start of the 5% H_2/Ar purge, the Pt-wire SE OCP decreased at a rate of $\sim 0.08 \text{ mV s}^{-1}$, approaching the Cu_{UPD} monolayer OCP of $0.40 \text{ V}_{\text{RHE}}$ within $\sim 2 \text{ h}$. As expected by the ~ 1.7 -fold lower amount of Pt surface exposed in the 20.0 wt% Pt/C catalyst, the time by which the Pt-wire SE OCP dropped to $0.40 \text{ V}_{\text{RHE}}$ was ~ 1.6 -fold faster than in the experiment with the 46.1 wt% Pt/C catalyst. However, this time the reaction was not stopped at $0.40 \text{ V}_{\text{RHE}}$ and was left to continue until the Pt-wire SE OCP reached an essentially steady-state value of $\sim 0.30 \text{ V}_{\text{RHE}}$ in order to evaluate the extent of the H_2 promoted Cu deposition on the Pt nanoparticles when left uninterrupted. This steady-state OCP of $\sim 0.30 \text{ V}_{\text{RHE}}$ had been identified above to closely represent the Cu^{2+}/Cu equilibrium potential on a bulk copper electrode. Consequently, it is not surprising that at this low OCP plateau shown in Fig. 11b, the formation of a thin orange band on the walls of the reaction cell just above the electrolyte surface could be seen (see photo in Fig. 11a). This can be explained by the much faster H_2 mass transport to Pt/C particles at the gas/electrolyte interface and in the electrolyte meniscus region, leading to a more rapid drop in the local potential of the Pt/C particles and thus to multi-layer copper plating, quite analogous to what had been observed for the H_2 promoted copper deposition on the Pt disk when using 100% H_2 (see Fig. 5a). After about one hour at the $\sim 0.30 \text{ V}_{\text{RHE}}$ OCP plateau, the electrolyte solution was filtrated and analyzed by UV-vis. A comparison of the

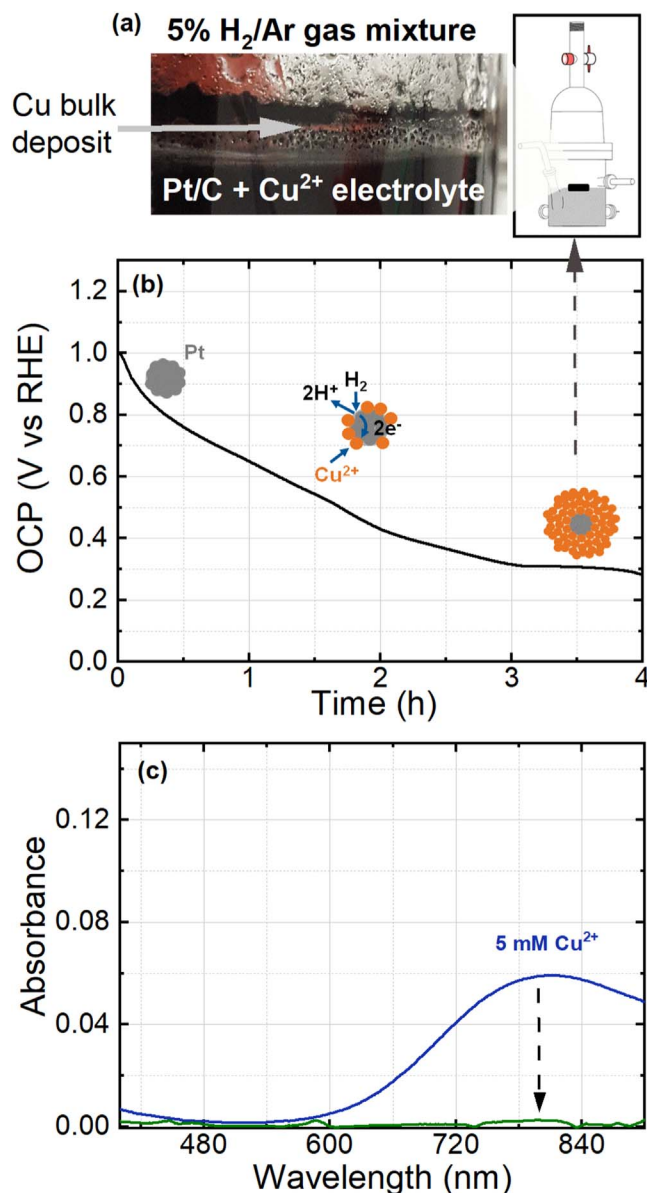


Figure 11. (a) Picture of the free electrolyte/gas interface in the reaction cell, showing the accumulation of the Pt/C catalyst outside of the electrolyte and the deposition of bulk Cu on the glass wall of the cell (pointed out by the arrow). (b) OCP transients of the Pt-wire sensing electrode in the presence of 0.5 g of a 20 wt% Pt/C catalyst dispersed in 110 ml of a 0.1 M $\text{HClO}_4 + 5 \text{ mM Cu}^{2+}$ electrolyte upon purging the initially air saturated electrolyte with 5% H_2/Ar , measured in the reaction cell (see Fig. 1a). (c) UV-Vis spectra of the as-prepared electrolyte with 5 mM Cu^{2+} in 0.1 M HClO_4 (blue) and of the filtrated electrolyte after 4 h, where the Pt-wire sensing electrode OCP has decreased to $\sim 0.3 \text{ V}_{\text{RHE}}$ (green). The sketches in (b) represent a simplified depiction of the copper deposition mechanisms at the different OCP values during the experiment.

UV-Vis spectra of the as-prepared electrolyte (blue line in Fig. 11c) and of the filtrated electrolyte after the experiment (green line) reveal an essentially complete consumption of the Cu^{2+} in the solution. Considering that 0.55 mmol Cu^{2+} were contained in the 110 ml of the 5 mM Cu^{2+} electrolyte and that the estimated moles of exposed Pt surface atoms in the reaction cell are $\sim 0.17 \text{ mmol}$, ~ 3.2 monolayer equivalents of copper were deposited on the catalyst in this experiment. This confirms that the H_2 promoted copper deposition in this reaction cell is clearly not self-limiting, and that this is due to the uncontrolled H_2 mass transport at the electrolyte/gas interface.

In summary, in contrast to the self-limiting copper monolayer deposition in the RDE experiments (see Figs. 7 and 9, respectively), in which the Pt disk and the thin-film electrodes were fully immersed in the electrolyte solution during the H₂ promoted deposition, the intermittent direct exposure of the dispersed Pt/C catalyst in our reaction cell (see Fig 1f) leads to uncontrolled H₂ mass transport and thus to an uncontrolled copper deposition. At the electrolyte/gas interface where the H₂ mass transport is very fast, copper bulk deposition occurs, analogous to what was observed in the case of the Pt disk experiment with 100% H₂. While the H₂ mass transport at the Pt-wire sensing electrode should remain well controlled and should in principle facilitate the formation of a Cu_{UPD} monolayer, a (partial) equilibration between Pt/C particles with Cu multi-layers and the sensing electrode also must lead to copper multi-layer deposition on the sensing electrode, as indicated by the fact that its potential also decreases to $\sim 0.30 V_{\text{RHE}}$ after a sufficiently long reaction time. Due to this complex interplay and due to the inhomogeneity of the copper deposition on the Pt/C particles, the OCP of the Pt-wire sensing electrode does not anymore serve as an indicator of the copper coverage of the Pt nanoparticles of the Pt/C catalyst. Thus, even if the reaction is interrupted at $0.40 V_{\text{RHE}}$, as in the example shown at Fig. 10, the amount of copper deposited on the Pt nanoparticles of the Pt/C catalyst already exceeds one monolayer. Even when the Cu²⁺ concentration in the electrolyte solution was limited to the exact number of moles required to form a Cu_{UPD} monolayer on the dispersed Pt/C catalyst, the deposition resulted in the copper bulk deposition on the Pt nanoparticles (experiments not shown). For this reason, in order to translate the self-limiting deposition characteristics observed for the RDE experiments and to assure the deposition of a uniform Cu monolayer on the Pt nanoparticles of the Pt/C material that would be needed for the large-scale preparation of, e.g., Cu-Pt near-surface alloys (NSAs) or core/ML shell catalysts, the deposition must be carried out in a reaction cell configuration that avoids the formation of a free electrolyte/gas interface, ensuring that all the Pt/C particles are always fully immersed in the electrolyte.

Conclusions

As an alternative to the commonly used electrochemical deposition methods, we developed an approach to form a self-limiting Cu_{UPD} monolayer on polycrystalline Pt electrodes and Pt/C catalysts, promoted solely by the introduction of a H₂ gas mixture into a Cu²⁺ containing electrolyte. The H₂ promoted Cu deposition reaction on Pt disk and Pt/C thin-film RDEs was monitored by OCP transients of the working electrode immersed in an initially air saturated Cu²⁺-containing electrolyte, whereby fast stripping voltammetry was used to quantify the amount of Cu deposited on the platinum surface. The initial evaluation of the method in the RDE configuration showed that the H₂ promoted Cu deposition under the described experimental conditions is driven by the reduction of the Cu²⁺ ions that is facilitated by the oxidation of H₂ on the Pt electrode. This is contrast to the H_{UPD} mechanism presented in other studies, where UPD hydrogen is suggested to react directly with Cu²⁺ ions.

By a comparison of the electrochemical deposition of UPD Cu via external potential control, we demonstrated that the Cu_{UPD} coverage at a given OCP is independent of whether the deposition is induced by the exposure to H₂ gas or by a cathodic deposition CV scan, as long as the final deposition potential and the effective rate of OCP decrease are comparable. For both deposition methods, the Cu_{UPD} onset was observed at potentials $< 0.80 V_{\text{RHE}}$ with the formation of a Cu monolayer established at $\sim 0.40 V_{\text{RHE}}$ for potential transients corresponding to $\sim 1 \text{ mV s}^{-1}$ and slower. We observed that the rate of the deposition reaction promoted by the H₂ gas is highly dependent on the local H₂ mass transport, and thus the concentration of H₂ in the gas mixture. Consequently, in order to assure the deposition of a full Cu_{UPD} monolayer, the H₂ concentration must be low enough to avoid OCP excursions to potentials near $\sim 0.30 V_{\text{RHE}}$, where the deposition of bulk Cu occurs. Once the H₂

promoted Cu_{UPD} monolayer on Pt is formed, the low activity of Cu for the HOR prevents any further reduction, evidenced by a steady-state OCP of $\sim 0.40 V_{\text{RHE}}$, rendering the Cu deposition process self-limiting.

In addition, based on the results obtained with the different evaluated Pt surfaces, the deposition method proposed here could be further adapted in the preparation of other noble metal core/ML shell nanoparticles supported on carbon. As long as the metal that is to be deposited has a standard reduction potential higher than the HOR/HER equilibrium potential, does form an underpotential deposition monolayer on the selected noble metal core, and has a low enough HOR activity to ensure a self-limiting deposition process.

In the second part of our work, we attempted the gram-scale H₂ promoted synthesis of a Cu_{UPD} monolayer on the Pt nanoparticles of a Pt/C catalyst to serve as the first steps towards the synthesis of Cu-Pt near-surface alloys (NSAs) or of core/ML-shell catalyst. However, the free electrolyte/gas interface present in the here designed reaction cell leads to uncontrolled and enhanced H₂ mass transport at this interface, thus resulting in the deposition of bulk Cu and compromising the self-limiting characteristics of the H₂ promoted deposition method. Therefore, the here pursued approach would require a cell design without a free electrolyte/gas interface where the dispersed Pt/C particles are always fully immersed, thereby ensuring the self-limiting formation of Cu_{UPD} monolayer.

Acknowledgments

We would like to gratefully acknowledge the funding by the International Graduate School of Science and Engineering (IGSSE) at the Technische Universität München—Project 11.01—ActiveElectroCat.

ORCID

Paulette A. Loichet Torres  <https://orcid.org/0000-0001-7304-9110>
 Hany A. El-Sayed  <https://orcid.org/0000-0002-8769-8258>
 Jan N. Schwämmlein  <https://orcid.org/0000-0001-8902-4508>
 Franziska Friedrich  <https://orcid.org/0000-0001-9400-1212>
 Hubert A. Gasteiger  <https://orcid.org/0000-0001-8199-8703>

References

- O. Gröger, H. A. Gasteiger, and J. P. Suchsland, *Journal of Electrochemical Society*, **162**, A2605 (2015).
- A. Kongkanand and M. F. Mathias, *The Journal of Physical Chemistry Letters*, **7**, 1127 (2016).
- B. Han, C. E. Carlton, A. Kongkanand, R. S. Kukreja, B. R. Theobald, L. Gan, R. O'Malley, P. Strasser, F. T. Wagner, and Y. Shao-Horn, *Energy Environ. Sci.*, **8**, 258 (2015).
- M. Escudero-Escribano, P. Malacrida, M. H. Hansen, U. G. Vej-Hansen, A. Velázquez-Palenzuela, V. Tripkovic, J. Schiøtz, J. Rossmeisl, I. E. L. Stephens, and I. Chorkendorff, *Science*, **352**, 73 (2016).
- R. Chattot, O. Le Bacq, V. Beermann, S. Kühn, J. Herranz, S. Henning, L. Kühn, T. Asset, L. Guétaz, G. Renou, J. Drnec, P. Bordet, A. Pastruel, A. Eychmüller, T. J. Schmidt, P. Strasser, L. Dubau, and F. Maillard et al., *Nat. Mater.*, **17**, 827 (2018).
- H. Lv, D. Li, D. Strmcnik, A. P. Paulikas, N. M. Markovic, and V. R. Stamenkovic, *Nano Energy*, **29**, 149 (2016).
- M. Shao, Q. Chang, J.-P. Dodelet, and R. Chenitz, *Chem. Rev.*, **116**, 3594 (2016).
- M. Escudero-Escribano, K. D. Jensen, and A. W. Jensen, *Current Opinion in Electrochemistry*, **8**, 135 (2018).
- R. R. Adzic and F. H. B. Lima, "Chapter 1: Platinum monolayer oxygen reduction electrocatalyst." *Handbook of Fuel Cells*, ed. W. Vielstich, H. Yokokawa, and H. Gasteiger (Wiley, New York, NY) **5**, 5 (2003).
- J. Zhang, F. H. B. Lima, M. H. Shao, K. Sasaki, J. X. Wang, J. Hanson, and R. R. Adzic, *The Journal of Physical Chemistry. B*, **109**, 22701 (2005).
- H. I. Karan, K. Sasaki, K. Kuttijiel, C. A. Farberow, M. Mavrikakis, and R. R. Adzic, *ACS Catal.*, **2**, 817 (2012).
- K. A. Kuttijiel, K. Sasaki, Y. Choi, D. Su, P. Liu, and R. R. Adzic, *Energy Environ. Sci.*, **5**, 5291 (2012).
- A. Kongkanand, N. P. Subramanian, Y. Yu, Z. Liu, H. Igarashi, and D. A. Muller, *ACS Catal.*, **6**, 1578 (2016).
- K. Sasaki, K. A. Kuttijiel, and R. R. Adzic, *Current Opinion in Electrochemistry*, **21**, 368 (2020).
- K. Sasaki, J. X. Wang, H. Naohara, N. Marinkovic, K. More, H. Inada, and R. R. Adzic, *Electrochim. Acta*, **55**, 2645 (2010).
- S. R. Brankovic, J. X. Wang, and R. R. Adzic, *Surf. Sci.*, **474**, L173 (2001).

17. A. S. Bondarenko, I. E. L. Stephens, and I. Chorkendorff, *Electrochem. Commun.*, **23**, 33 (2012).
18. A. S. Bandarenka, A. S. Varela, M. Karamad, F. Calle-Vallejo, L. Bech, F. J. Perez-Alonso, J. Rossmeisl, I. E. L. Stephens, and I. Chorkendorff, *Angewandte Chemie (International ed. in English)*, **51**, 11845 (2012).
19. A. S. Bondarenko, I. E. L. Stephens, L. Bech, and I. Chorkendorff, *Electrochim. Acta*, **82**, 517 (2012).
20. I. E. L. Stephens, A. S. Bondarenko, F. J. Perez-Alonso, F. Calle-Vallejo, L. Bech, T. P. Johansson, A. K. Jepsen, R. Frydendal, B. P. Knudsen, J. Rossmeisl, and I. Chorkendorff, *JACS*, **133**, 5485 (2011).
21. M. B. Vukmirovic, J. Zhang, K. Sasaki, A. U. Nilekar, F. Uribe, M. Mavrikakis, and R. R. Adzic, *Electrochim. Acta*, **52**, 2257 (2007).
22. S. Szabó and F. Nagy, *J. Electroanal. Chem.*, **70**, 357 (1976).
23. S. Szabó, *J. Electroanal. Chem.*, **77**, 193 (1977).
24. S. Szabo and F. Nagy, *J. Electroanal. Chem.*, **87**, 261 (1978).
25. S. Szabo and F. Nagy, *J. Electroanal. Chem.*, **85**, 339 (1977).
26. S. Szabó, I. Bakos, and F. Nagy, *J. Electroanal. Chem.*, **263**, 137 (1989).
27. F. J. Vidal-Iglesias, A. Al-Akl, D. J. Watson, and G. A. Attard, *Electrochem. Commun.*, **8**, 1147 (2006).
28. M. J. Llorca, J. M. Feliu, and A. Aldaz, *J. Electroanal. Chem.*, **351**, 299 (1993).
29. R. Gomez, A. Rodes, J. M. Perez, J. M. Feliu, and A. Aldaz, *Surf. Sci.*, **327**, 202 (1995).
30. J. M. Dumas, C. Géron, H. Hadrane, P. Marécot, and J. Barbier, *J. Mol. Catal.*, **77**, 87 (1992).
31. E. A. Redina, O. A. Kirichenko, A. A. Greish, A. V. Kucherov, O. P. Tkachenko, G. I. Kapustin, I. V. Mishin, and L. M. Kustov, *Catal. Today*, **246**, 216 (2015).
32. J. Margitfalvi, S. Szabó, and F. Nagy, "Supported Bimetallic Catalysts Prepared by Controlled Surface Reactions." *Stud. Surf. Sci. Catal. (Elsevier, New York, NY) Catalytic hydrogenation*, **27**, 373 (1986).
33. F. Taufany et al., *ACS Nano*, **5**, 9370 (2011).
34. T. Mittermeier, A. Weiß, H. A. Gasteiger, and F. Hasché, *J. Electrochem. Soc.*, **164**, F1081 (2017).
35. C. L. Green and A. Kucernak, *J. Phys. Chem. B*, **106**, 1036 (2002).
36. N. M. Marković, H. A. Gasteiger, and P. N. Ross Jr., *Langmuir*, **11**, 4098 (1995).
37. K. Varga, P. Zelenay, and A. Wieckowski, *J. Electroanal. Chem.*, **330**, 453 (1992).
38. S. A. S. Machado, A. A. Tanaka, and E. R. Gonzalez, *Electrochim. Acta*, **36**, 1325 (1991).
39. N. Markovic and P. N. Ross, *Langmuir*, **9**, 580 (1993).
40. L. W. H. Leung, T. W. Gregg, and D. W. Goodman, *Langmuir*, **7**, 3205 (1991).
41. S. H. Cadle and S. Bruckenstein, *Anal. Chem.*, **43**, 1858 (1971).
42. S. Szabó, *Int. Rev. Phys. Chem.*, **10**, 207 (1991).
43. A. J. Bard, R. Parsons, and J. Jordan, *Standard Potentials in Aqueous Solutions (IUPAC—CRC Press, New York, NY)* 292 (1985).
44. A. G. Zelinsky, B. Y. Pirogov, and O. A. Yurjev, *Corros. Sci.*, **46**, 1083 (2004).
45. J. Durst, C. Simon, F. Hasché, and H. A. Gasteiger, *J. Electrochem. Soc.*, **162**, F190 (2015).
46. H. H. Perkampus, *UV-vis Spectroscopy and its Applications* (Springer, Berlin) 27 (1992).